

## **General Disclaimer**

### **One or more of the Following Statements may affect this Document**

- This document has been reproduced from the best copy furnished by the organizational source. It is being released in the interest of making available as much information as possible.
- This document may contain data, which exceeds the sheet parameters. It was furnished in this condition by the organizational source and is the best copy available.
- This document may contain tone-on-tone or color graphs, charts and/or pictures, which have been reproduced in black and white.
- This document is paginated as submitted by the original source.
- Portions of this document are not fully legible due to the historical nature of some of the material. However, it is the best reproduction available from the original submission.

# NASA TECHNICAL MEMORANDUM

NASA TM X-64972

## A MINIATURIZED POINTING MOUNT FOR SPACELAB MISSIONS

(NASA-TM-X-64972) A MINIATURIZED POINTING  
MOUNT FOR SPACELAB MISSIONS (NASA) 69 p HC  
\$4.50 CSCL 14B

N76-15261

Unclas

G3/19 08591

By Carl G. Fritz, Joe, T. Howell, Jr.,  
P. D. Nicaise, and Joe R. Parker  
Preliminary Design Office

November 25, 1975



**NASA**

*George C. Marshall Space Flight Center  
Marshall Space Flight Center, Alabama*

1. REPORT NO. NASA TM X- 64972		2. GOVERNMENT ACCESSION NO.		3. RECIPIENT'S CATALOG NO.	
4. TITLE AND SUBTITLE  A Miniaturized Pointing Mount for Spacelab Missions				5. REPORT DATE November 25, 1975	
				6. PERFORMING ORGANIZATION CODE	
7. AUTHOR(S) Carl G. Fritz, Joe T. Howell, Jr., P. D. Nicaise, and Joe R. Parker				8. PERFORMING ORGANIZATION REPORT #	
9. PERFORMING ORGANIZATION NAME AND ADDRESS  George C. Marshall Space Flight Center Marshall Space Flight Center, Alabama 35812				10. WORK UNIT NO.	
				11. CONTRACT OR GRANT NO.	
12. SPONSORING AGENCY NAME AND ADDRESS  National Aeronautics and Space Administration Washington, D. C. 20546				13. TYPE OF REPORT & PERIOD COVERED  Technical Memorandum	
				14. SPONSORING AGENCY CODE	
15. SUPPLEMENTARY NOTES  Prepared by Preliminary Design Office, Program Development.					
16. ABSTRACT  A Miniaturized Pointing Mount (MPM) for Spacelab missions is defined and simulation results are described. This mount is proposed to complement the Spacelab Instrument Pointing System (IPS) as developed by the Europeans. It uses the same mount isolator concept as the Spacelab IPS but is much more efficient and economical for the accommodation of small Shuttle payloads. The MPM is built from star tracker assemblies left over from the Apollo Telescope Mount program thereby assuring low cost and development risk. Simulation results indicate a high level of instrument stability can be expected. The short development time of the MPM would permit it to serve as a precursor to the Spacelab IPS for verifying critical new concepts such as the mount isolation and hold down mechanisms.					
17. KEY WORDS  Pointing mount Instrument pointing Instrument stability Low cost			18. DISTRIBUTION STATEMENT  Unclassified — Unlimited		
19. SECURITY CLASSIF. (of this report)  Unclassified	20. SECURITY CLASSIF. (of this page)  Unclassified		21. NO. OF PAGES  68	22. PRICE  NTIS	

# TABLE OF CONTENTS

	Page
I. INTRODUCTION . . . . .	1
II. THE MOUNT ISOLATOR CONCEPT . . . . .	3
III. MINIATURIZED POINTING MOUNT DEFINITION . . . . .	4
IV. SENSORS . . . . .	10
V. SIMULATION MODEL . . . . .	13
VI. SIMULATION RESULTS . . . . .	20
VII. THERMAL CONTROL SYSTEMS . . . . .	21
VIII. PRELAUNCH TEST AND VERIFICATION PHILOSOPHY . . . . .	39
IX. CONCLUSIONS AND RECOMMENDATIONS . . . . .	46
APPENDIX A: STAR TRACKER FOR THE APOLLO TELESCOPE MOUNT . . . . .	41
APPENDIX B: DYNAMIC MODEL . . . . .	48
APPENDIX C: COMPUTER OUTPUT . . . . .	51



# LIST OF ILLUSTRATIONS

Figure	Title	Page
I-1.	Comparison of Miniaturized Pointing Mount with Spacelab IPS . . . . .	2
III-1.	Modifications to the ATM Star Tracker . . . . .	5
III-2.	Stowage concept for the MPM . . . . .	8
III-3.	Miniaturized Pointing Mount control system concept . . . . .	9
III-4.	Pallet mounted Miniaturized Pointing Mount . . . . .	10
III-5.	Boom tip MPM . . . . .	11
III-6.	Airlock MPM . . . . .	12
III-7.	Deployed airlock MPM . . . . .	13
V-1.	Simulation model . . . . .	17
V-2.	System flow diagram . . . . .	19
V-3.	Man motion design profile . . . . .	20
VI-1.	MPM pointing performance for 130 kg instrument . . . . .	22
VI-2.	MPM pointing performance for 500 kg instrument . . . . .	23
VI-3.	MPM slewing and tracking performance . . . . .	24
VII-1.	MPM thermal control concept . . . . .	27
VII-2.	MPM thermal control schematic . . . . .	28
VII-3.	Thermal model relative mounting position . . . . .	29
VII-4.	Significant temperatures on thermal model with payload bay and MPM canister solar oriented (radiator area is 1.92 m <sup>2</sup> ) . . . . .	31

## LIST OF ILLUSTRATIONS (Continued)

Figure	Title	Page
VII-5.	Significant temperatures on thermal model with payload bay and MPM canister pointed to the local vertical ( radiator area is 1.92 m <sup>2</sup> ) . . . . .	32
VII-6.	Significant temperatures on thermal model with payload bay normal axis oriented 30° off the solar vector and MPM pointed toward the sun ( radiator area is 1.92 m <sup>2</sup> ) . . . . .	33
VII-7.	Significant temperatures on thermal model with payload bay and MPM canister facing 90° from solar vector ( radiator area is 1.92 m <sup>2</sup> ) . . . . .	34
VII-8.	Significant temperatures on thermal model with payload bay and MPM canister oriented toward the sun ( radiator area is 0.92 m <sup>2</sup> ) . . . . .	35
VII-9.	Typical entry profile . . . . .	36
VII-10.	Pump power, weight, and radiator area as a function of temperature difference between radiator and inside wall limits . . . . .	37
A-1.	Star tracker optical-mechanical assembly . . . . .	42
A-2.	Flex lead configuration . . . . .	44
A-3.	Block diagram of ATM Star Tracker gimbal servo system . .	46
B-1.	Three-body planar model . . . . .	50
C-1.	Dynamic response for 100 N/m shock mount stiffness . . . . .	53
C-2.	Dynamic response for 250 N/m shock mount stiffness . . . . .	54
C-3.	Dynamic response for 10 <sup>5</sup> N/m shock mount stiffness . . . . .	55

## LIST OF ILLUSTRATIONS (Concluded)

Figure	Title	Page
C-4.	Dynamic response for 100 N/m shock mount stiffness . . . . .	56
C-5.	Dynamic response for 250 N/m shock mount stiffness . . . . .	57
C-6.	Dynamic response for $10^5$ N/m shock mount stiffness . . . . .	58
C-7.	Slow and fast tracking for the small experiment . . . . .	59
C-8.	Slow and fast tracking for the large experiment . . . . .	60

# LIST OF TABLES

Table	Title	Page
III-1.	Miniaturized Pointing Mount Characteristics — Basic ATM Star Tracker Application . . . . .	7
IV-1.	Gyros . . . . .	14
IV-2.	Star Trackers . . . . .	15
IV-3.	Sun Sensors . . . . .	16
V-1.	Summary of Mass Characteristics . . . . .	17
V-2.	Summary of MPM Characteristics . . . . .	18
VII-1.	MPM Instrument Characteristics . . . . .	25
VII-2.	MPM Thermal Control System Weight . . . . .	38

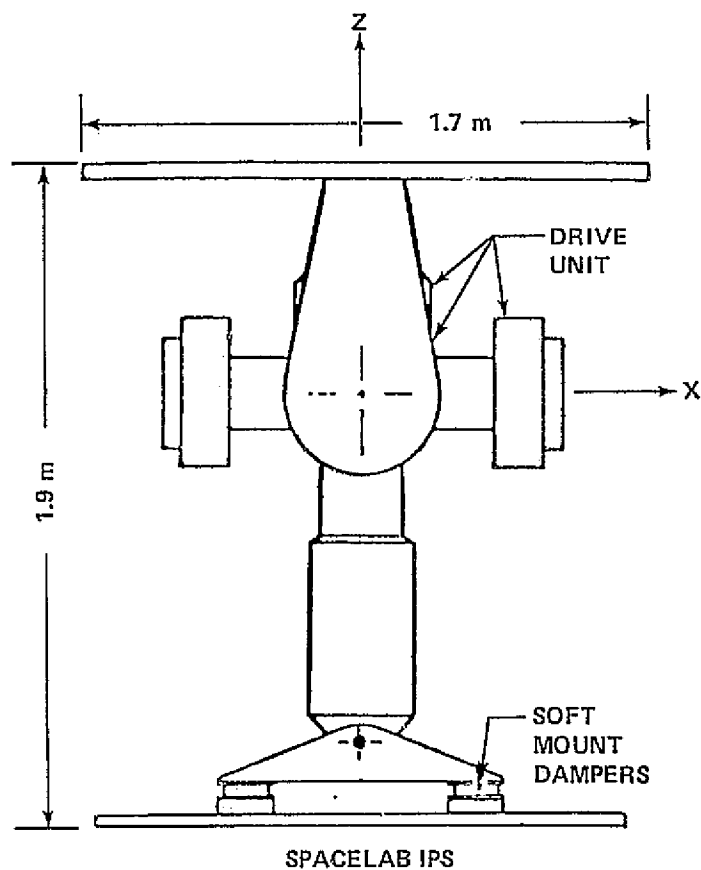
## A MINIATURIZED POINTING MOUNT FOR SPACELAB MISSIONS

### I. INTRODUCTION

The Spacelab sortie missions are planned to accommodate a number of scientific experiments during a limited time in earth orbit. Experiments are carried to orbit by the Shuttle and remain in the payload bay for an interval of several days before return. This mode permits individual experiments to make use of Shuttle and Spacelab power, communications, data processing, thermal control, and stabilization equipment. The stabilization equipment for the many different telescopes will include a general purpose experiment mount developed by the European Space Agency (ESA). This Instrument Pointing System (IPS) is planned to accommodate a wide variety of experiments up to the largest instruments that can be carried aboard the Shuttle. A Miniaturized Pointing Mount (MPM) is proposed that would complement the IPS by providing a number of services for which the IPS is not especially suited. NASA TM X-64896, "An Assessment of the Instrument Pointing Subsystems (IPS) Requirements for Spacelab Missions," defines small instrument requirements. These functions include operation from within the airlock, boom tip pointing, antenna control, and pointing of many small instruments that are flown on a space-available basis.

The MPM is being developed to provide these functions as a general purpose small instrument mount with minimum size, weight, and cost. Figure I-1 shows the MPM size in comparison to the IPS. The MPM is assured of minimum cost and development risk, because it can be built by the modification of existing hardware. Star tracker assemblies left over from the Apollo Telescope Mount (ATM) program are available for conversion into enough small, high quality instrument mounts to satisfy the Spacelab program for many years.

The MPM will incorporate new disturbance isolation techniques planned for the IPS. A combination of spring isolation and high speed controllers achieves high accuracy pointing without mass balancing of experiments. Older concepts require precision balancing of experiments and near ideal gimbal



ITEM	ESRO IOG	MPM
PAYLOAD WEIGHT	5000 kg	500 kg
MOUNT WEIGHT	700 kg	56 kg

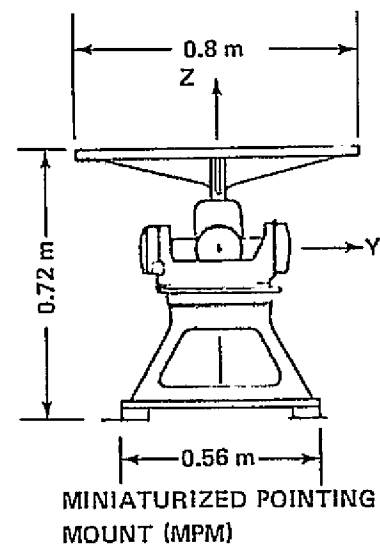


Figure I-1. Comparison of Miniaturized Pointing Mount with Spacelab IPS.

bearings to reach a comparable level of performance. These previous concepts were simply extensions of earth-based telescope mounts and suffer from very high mount-to-payload-weight ratio constraints on experiment shape and inherent high cost. The MPM (and the European Inside Out Gimbal) can carry payloads that are many times heavier than the mount and are relatively insensitive to payload shape, size, or location of experiment center of mass. High levels of stability can even be maintained during changes in center of mass that result from repositioning of fluids or film within the experiment.

The short development time of the MPM should allow it to serve the orbital flight test (OFT) missions that precede Spacelab missions. A most valuable service during these early missions is to verify the isolation technique for the IPS and demonstrate that adequate performance is possible on orbit. Performance testing of the isolators in a gravity environment is not completely satisfactory. Therefore, it is extremely critical that a precursor to the IPS be available to test this technique before the entire Spacelab instrument complement is committed to the IPS. A major factor in this early testing would be to build experimenter confidence in the IPS and prevent excessive development of alternative pointing equipment.

## II. THE MOUNT ISOLATOR CONCEPT

The stability of a pointed instrument is a function of the disturbances, translation and rotational isolation, structural stiffness, noise of the sensors, and controller effectiveness. Disturbances to Shuttle-attached experiments are significantly higher than those for free flyers primarily because of crew motion and thruster firings. Therefore, design of an experiment mount to achieve high levels of stability for sortie missions is especially difficult.

Conventional experiment mounts minimize translational coupling by precise balancing of experiment mass to coincide with the gimbal axes. An alternate technique, which has been selected for the European IPS, is the light spring isolator concept. The secret of this concept is not the inside-out gimbal order chosen by the Europeans but the limited rotational and translational freedom of the mount pedestal permitted by the isolators. The isolators attenuate external disturbances to the mount and change the characteristics of the disturbance waveform. The isolators serve as a low pass filter which transmits only those waveforms that are easily corrected by the controller.

The primary advantages of the isolator concept are (1) no precise mass balancing of experiments, (2) insensitivity to mass changes within the experiment, (3) insensitivity to pallet or Shuttle structural stiffness, and (4) freedom to reconfigure gimbal axis geometry for minimum size, weight, and cost. There are also certain inherent disadvantages to this concept such as (1) degradation of accuracy for large gimbal angles relative to the vertical, (2) the mount must be caged during boost and reentry, (3) end mounting of large experiments requires a stiff interface and results in large swept volumes, (4) slewing of large payloads may result in excessive deflection of the isolators, (5) sensor location on the instrument may be required to minimize interface stiffness, and (6) preflight performance verification will be restricted.

In spite of the potential disadvantages, the spring isolator concept shows great promise. The freedom to move the gimbal axes away from the experiment center of mass not only does away with inherently heavy girth rings, yokes, or ballast but also permits the use of a relatively small gimbal set. Now the advantages begin to become obvious. The small gimbals permit small bearing diameters and reduced friction for conventional ball bearings. The single bearing system rather than a coarse plus a fine bearing now becomes a real possibility. Since the gimbal set does not constrain the payload and gimbal order is somewhat arbitrary, the use of an existing gimbal system is the next obvious step.

### III. MINIATURIZED POINTING MOUNT DEFINITION

The ATM Star Tracker, which is described in Appendix A, has a set of gimbals with high quality bearings that are well suited to this application. Figure III-1 shows the modifications required to convert existing ATM hardware into a baseline MPM. The baseline MPM contains only those changes that are necessary to produce a practical pointing system. Additional changes that would increase performance are reserved for discussion later.

The baseline changes include the following: (1) removal of Star Tracker optics; (2) addition of a roll gimbal, roll gimbal torquer, and resolver; (3) addition of a pedestal with light spring isolators and stowage locks; (4) modification of the electronics assembly; and (5) addition of an experiment base plate or mounting structure. The roll capability is included in this baseline because of the large number of experiments that require roll stability to prevent smear at



STAR TRACKER OPTICS

EXPERIMENT BASE PLATE

TYPICAL

ROLL GIMBAL DRIVE

STAR TRACKER FRAME AND GIMBALS

PEDESTAL

STOWAGE LOCKS

ISOLATORS

Figure III-1. Modifications to the ATM Star Tracker.

the edge of the field. The torquer for the roll axis can be the same type as the existing 0.6 N-m torque motors. However, torque motors with 1.4 N-m capability would fit in the existing space. These motors are available off-the-shelf and would improve performance potential. A resolver is proposed for angular readout in place of the existing encoder to provide coordinate transformation for the middle and outer gimbals. Resolvers with a resolution of  $0.1^\circ$  are available that will fit within the available space. The pedestal is planned as a simple mechanical structure that would provide a mounting surface for the Star Tracker frame. The pedestal would interface to the pallet through the light spring isolators and a set of stowage locks. The same type of isolators could be used as are being developed for the Spacelab IPS. Changes to the electronics assembly include the addition of new circuit boards for driving the roll torquer and processing the roll gimbal readout. There is sufficient room in the existing box for these additions.

These changes to the existing ATM Star Tracker result in an MPM as defined in Table III-1. The MPM is expected to accommodate payloads of 1 m diameter by 3 m length with a mass of approximately 500 kg. The gimbal arrangement permits  $90^\circ$  rotation into the stowed position. The inner gimbal is aligned with the experiment long axis, thereby producing pure roll about line of sight. This MPM structure is adequate for orbital operations, but the mount and payload must be securely stowed during ascent and reentry. The stowage procedure is the same as that planned for the Spacelab IPS. The experiment base plate temporarily detaches from the mount to allow independent stowage of the payload. The mount is latched firmly to the pallet by electromechanical actuators. This stowage concept is shown in Figure III-2.

The MPM is planned to be largely independent of Spacelab data processing. A dedicated mini-processor (MP) is integrated with the MPM to provide all essential computational and logic commands for the pointing and control system. A block diagram of the system is shown in Figure III-3. Most sensor outputs are available in a digital format that is acceptable by the MP. The roll tracker is optional and will not be necessary for many payloads. Roll stability can usually be maintained by gyro reference alone. Sensor details are described in Section IV. The MP is also expected to accept commands directly from a sensor integral to the experiment and to compute drive commands for secondary mirror control. Interface with the Spacelab computer will be through a remote acquisition unit (RAU) dedicated to the MPM. The extent of this interface will depend largely on the payload operational requirements. For instance, this interface may be used only for simple mode commands such as deploy, start

TABLE III-1. MINIATURIZED POINTING MOUNT CHARACTERISTICS — BASIC  
ATM STAR TRACKER APPLICATION

Predicted Performance	Capabilities	Requirements
Payload Weight/ Size	Up to 500 kg/1 m x 3 m	Instruments 370 kg/1 m diameter
Pointing Accuracy/Stability	1 arc s/1 arc s	1 arc s/1 arc s
Gimbal Range	±90° outer ±50° middle ±180° roll	±70° line of sight travel ±90° launch tie-down
Torque Capability	0.6 N-m all axes	
Slewing Capability	-Satisfactory for stellar target changing -Satisfactory for most earth observation missions -Some limitations for fixed earth targets (i.e., 310 km, 500 kg; P/L, 1.5°/s)	Target to target change (LST type capability 90°/10 min) Horizon to horizon track
<u>Design Elements/Weight</u>	<u>Weight</u>	
Two Motor/Tach Assemblies	3.18	Weight consistent with size for airlock
Two Encoders	3.88	
Frame/Gimbal/		
Miscellaneous Parts	14.66	
Electronics Box	32.50	
Roll Gimbal/Experiment Base	30	
Pedestal/Isolators	40	
	124 (56 kg)	

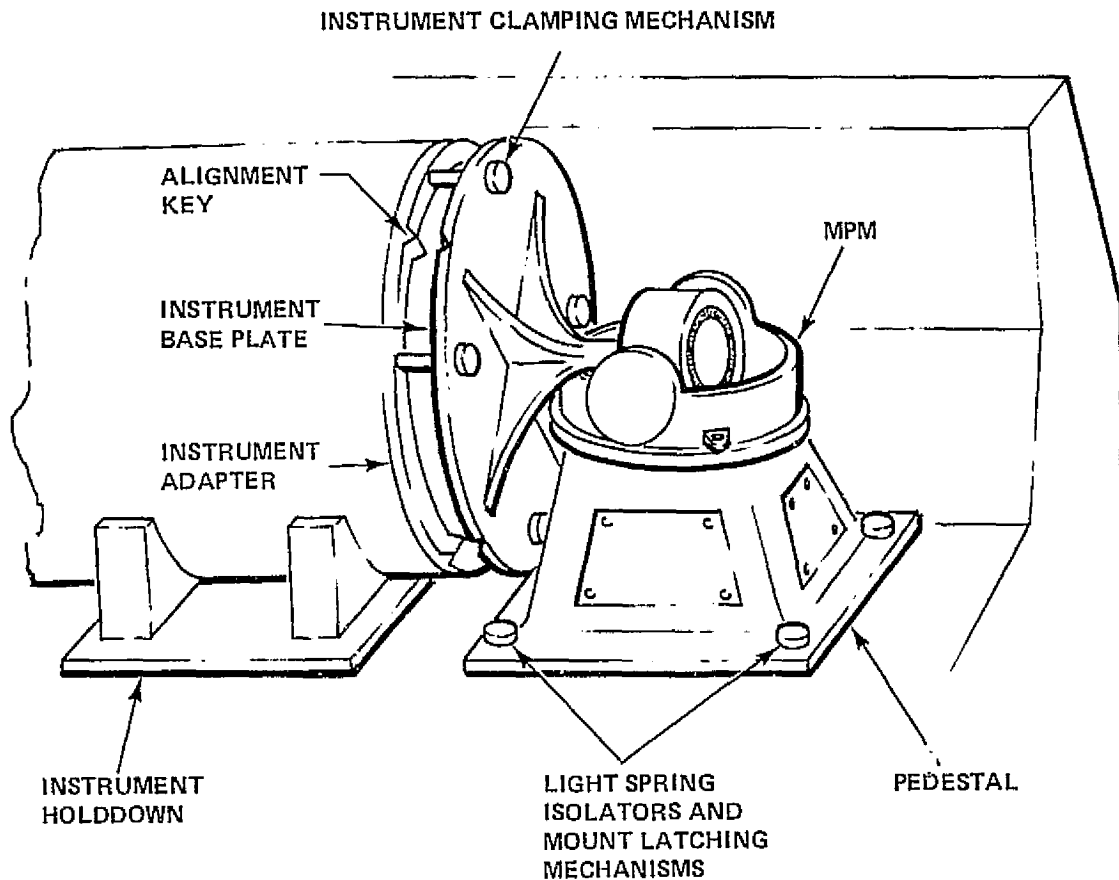


Figure III-2. Stowage concept for the MPM.

search, and stow. These commands must be input either from the ground, crew, or Spacelab computer that has knowledge of a Shuttle status. The data transfer through the RAU could be expanded to carry Shuttle state vector, ephemeris data on targets, and manual drive commands from the payload specialist station.

The MPM gimbal drive system is designed to be inherently stable for any loss of signal or drive command. The high speed control circuits are closed through the analog electronics assembly with a gyro reference. The MP controls the gimbals indirectly by reorientation of the reference gyros. Provisions can be made for direct manual drive of the gimbal torquers in case of complete failure of the MP or gyros. Besides the advantages of inherent stability and isolation of all high speed functions from the digital processor, this design reduces the command signal fluctuations that result from sensor sample rate.

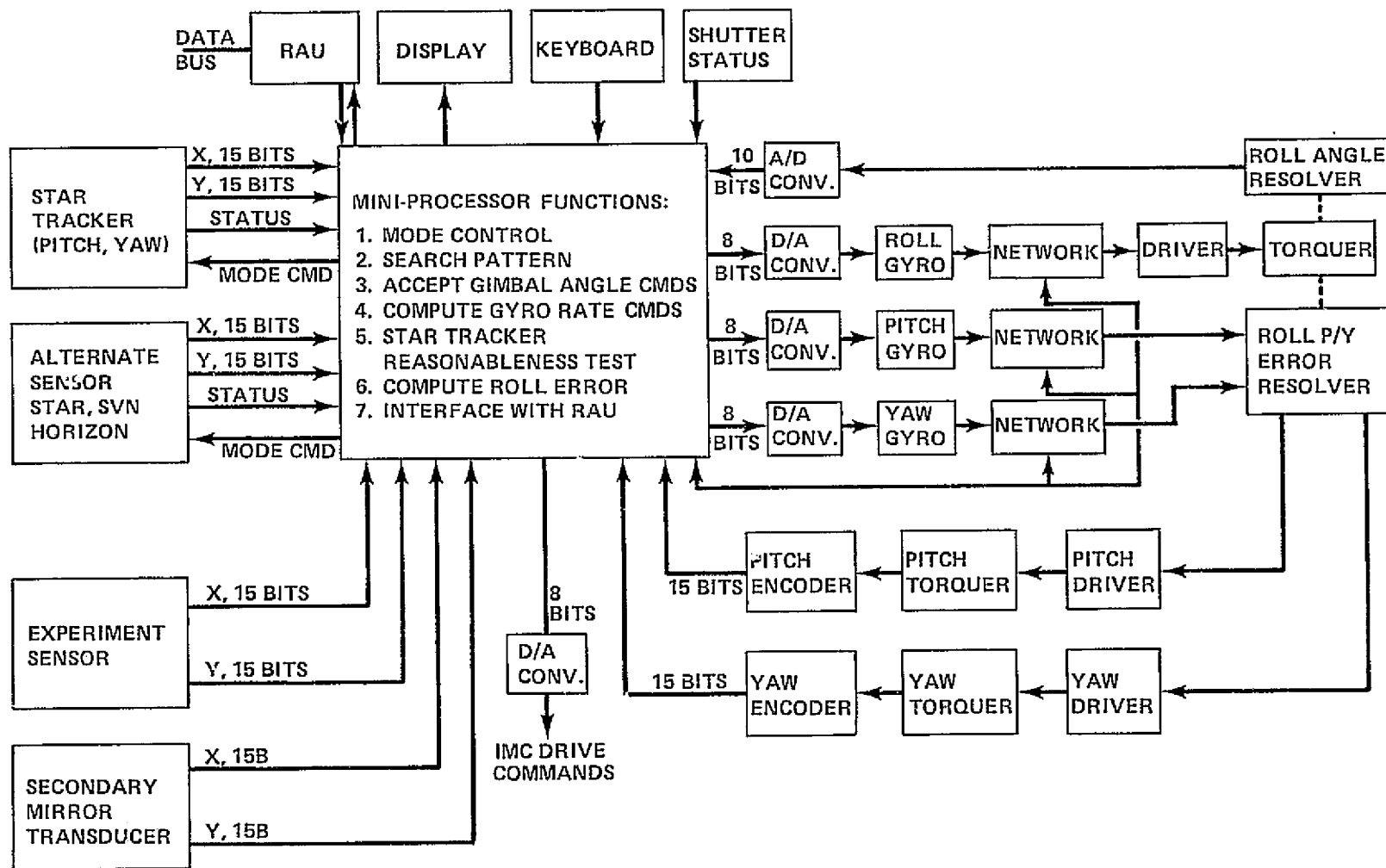


Figure III-3. Miniaturized Pointing Mount control system concept.

Typical instrument pointing using an MPM mounted on the Spacelab pallet is illustrated in Figure III-4. Figure III-5 illustrates the MPM in a boom tip pointing mode while Figures III-6 and 7 show the MPM as configured for airlock operation.

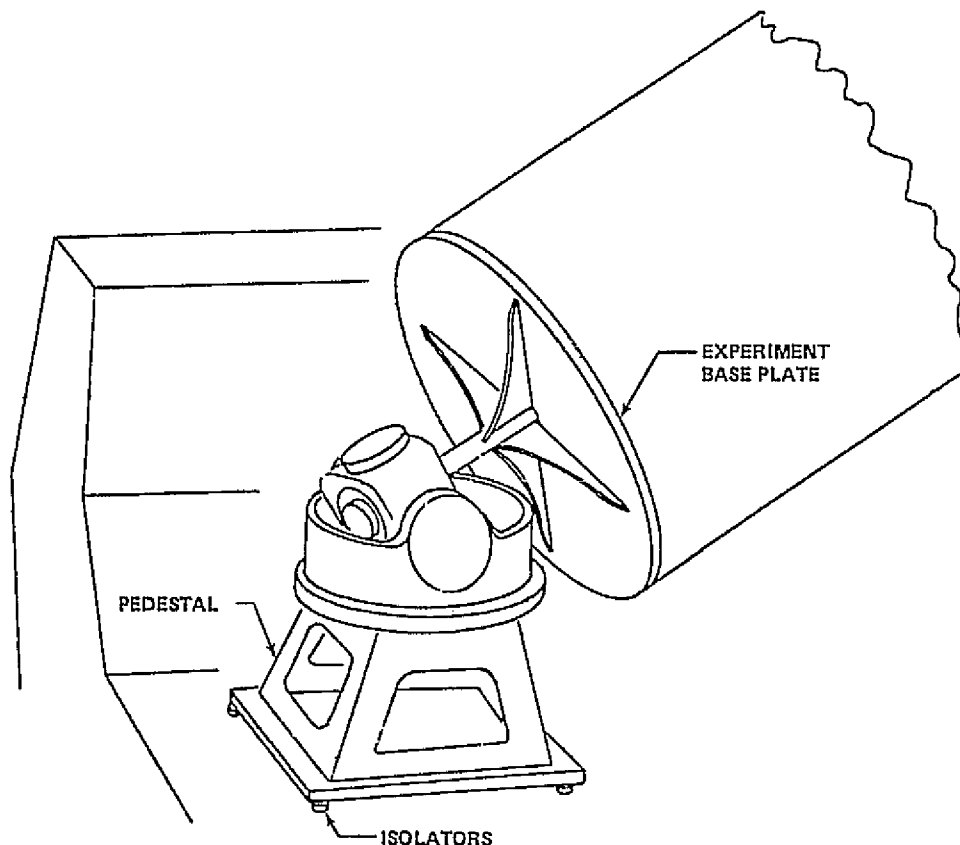


Figure III-4. Pallet mounted miniaturized pointing mount.

## IV. SENSORS

Pointing information to the MPM control system may be derived from many types of sensors. The primary mode of operation, shown for stellar operation in Figure III-3, consists of a reference gyro for each axis with appropriate updates from additional sensors. These additional sensors may be star trackers, sun sensors, or earth sensors depending on the particular experiment requirements. Flexibility in selecting control sensors is necessary

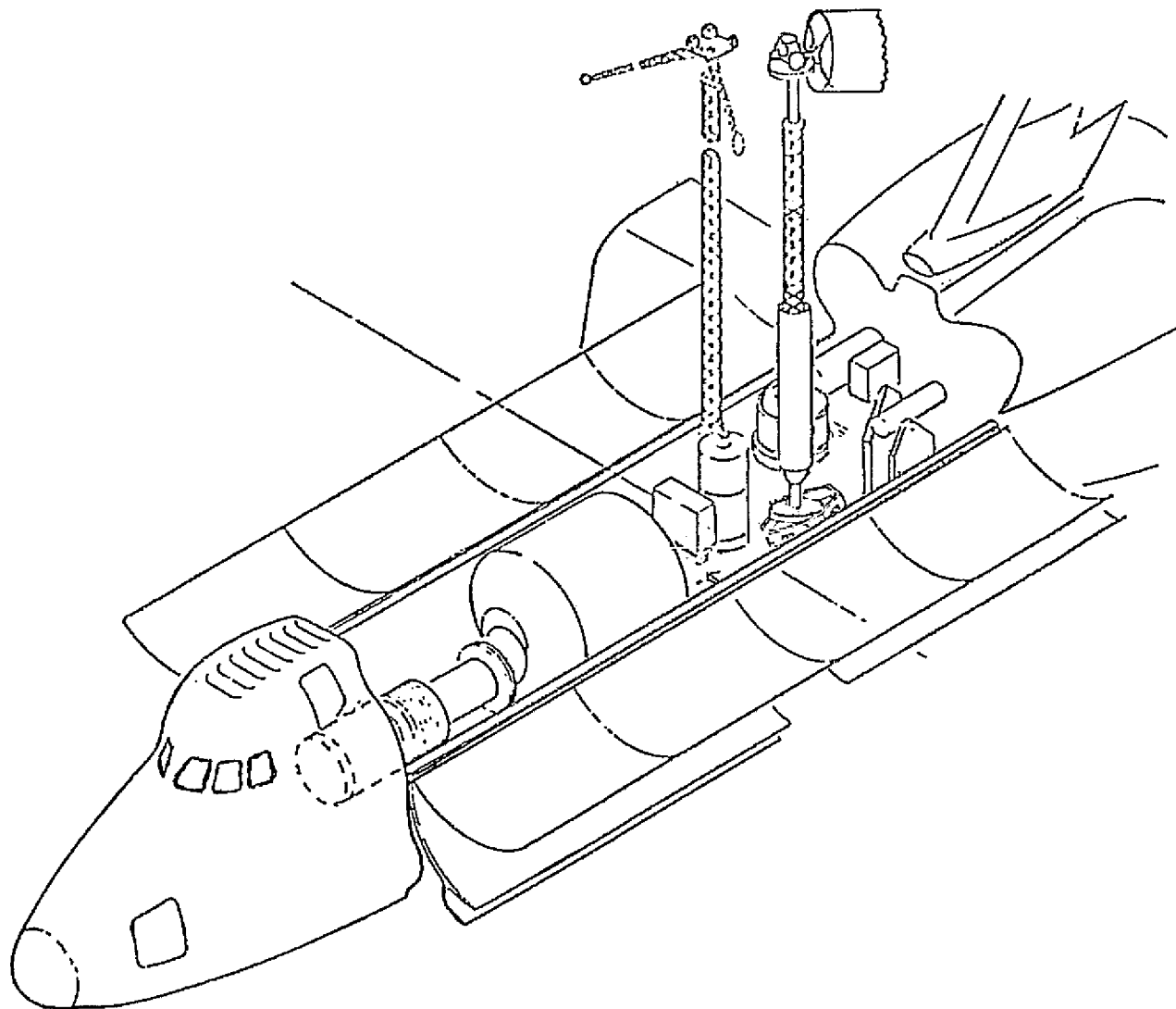


Figure III-5. Boom tip MPM.

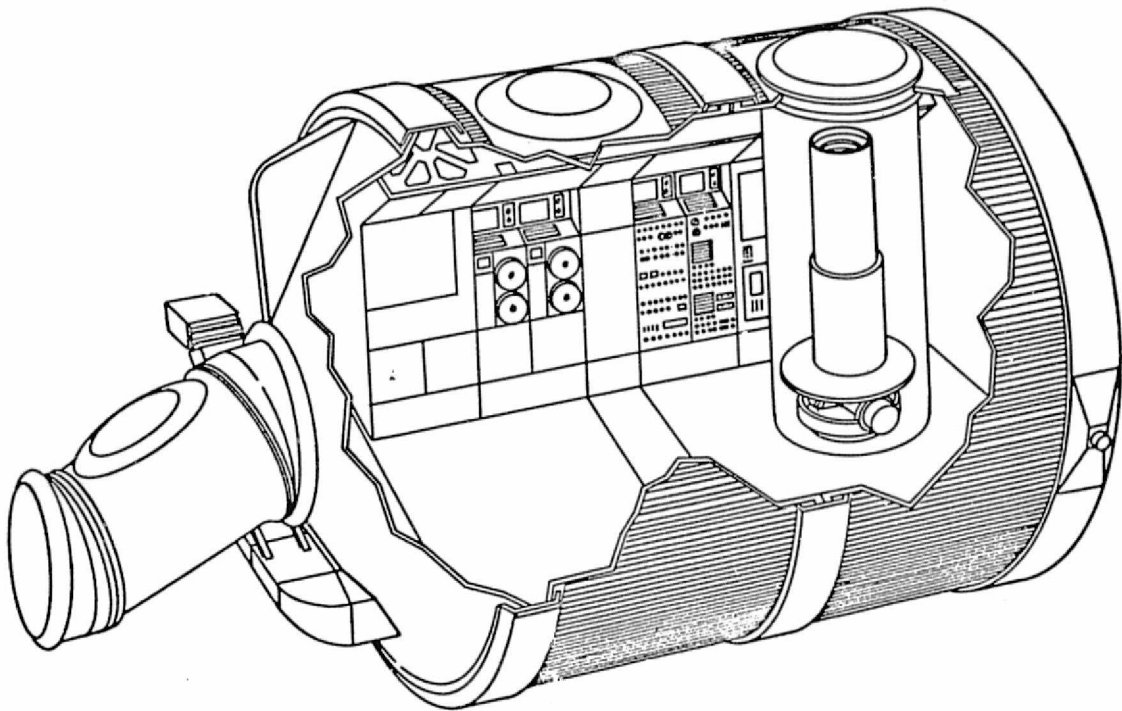


Figure III-6. Airlock MPM.

to accommodate the wide variety of experiments anticipated. Conceivably, the mount could be controlled by gyros only if the experiment has loose tolerances. A finely pointed system may require a reference signal from the experiment to provide the more stringent levels of control. Tables IV-1, IV-2, and IV-3 list gyros, star trackers, and sun sensors, respectively, which may be considered for use on the MPM.

A typical control system may consist of two tuned rotor (dry) gyros, and two HEAO-B Star Trackers for stellar and earth observations. For solar pointing, a sun sensor may be added. Fine pointing to earth targets is perhaps the most difficult task from a sensing standpoint. Horizon sensors, landmark trackers, correlation trackers, and others have been proposed. Each offers some advantages but does not adequately meet all requirements. The typical system discussed here with Shuttle-provided navigation and ephemeris data to determine the required pointing direction is more desirable for most earth-oriented experiments.



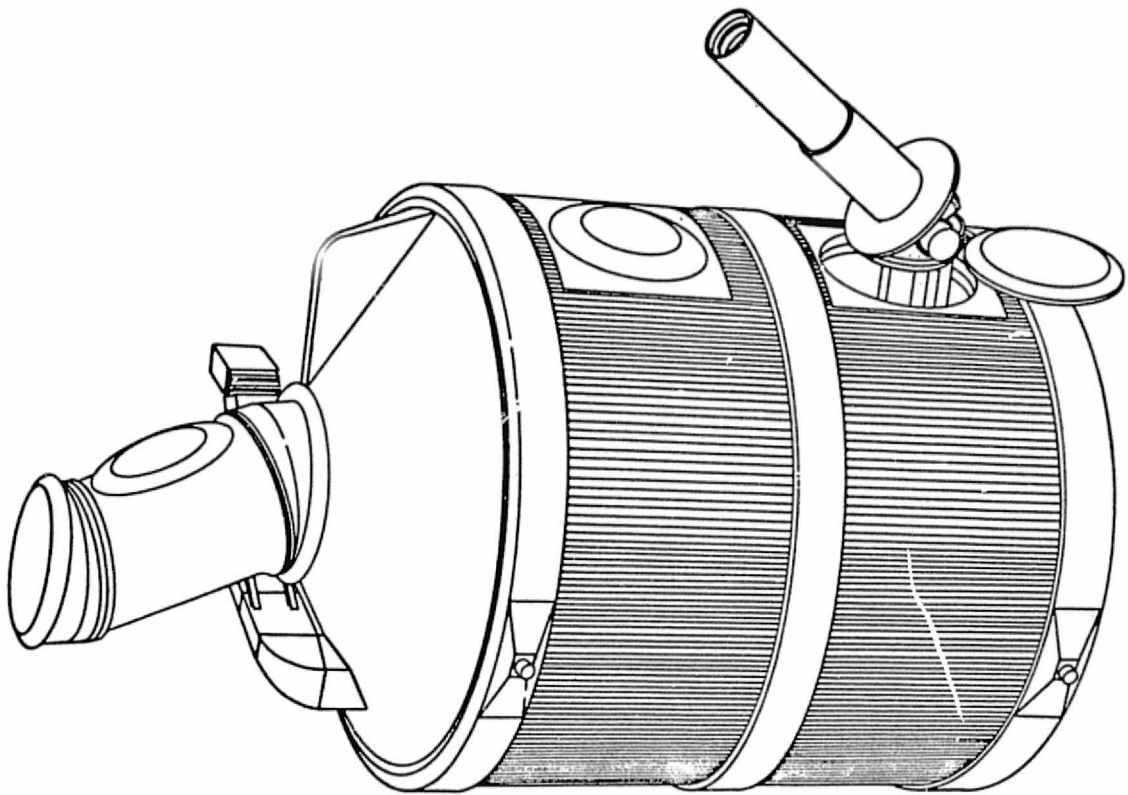


Figure III-7. Deployed airlock MPM.

## V. SIMULATION MODEL

The simulation model of the MPM consists of three bodies as depicted in Figure V-1. The Shuttle and pedestal were connected by a set of isolators, while the pedestal and experiment were connected by a gimbal. The dynamic equations of motion were developed and simplified for the simulation model. A complete list of equations is given in Appendix B. A summary of Shuttle, pedestal, and experiment characteristics is given in Table V-1. Two experiments were used in the simulation model, one being the Schwarzschild camera as a typical experiment and the other being a larger package depicting a maximum payload. Other parameters used in the simulation are given in Table V-2.

TABLE IV-1. GYROS

Manufacturer	Model No.	Type	Random Drift	Noise	Status
Bendix	LDG-540	Single-degree-of-freedom, freon floated, rate integrating gyro.	$0.005^\circ/\text{h}$ , $1\sigma$	0.0025 arc s	Development
	64 PMRIG	High precision, single-degree-of-freedom, rate integrating gyro.	$0.001^\circ/\text{h}$	$0.144^\circ/\text{h}$ (rms) 0 to 2.5 Hz $0.192^\circ/\text{h}$ 0 to 3.75 Hz $0.245^\circ/\text{h}$ 0 to 5.0 Hz $0.808^\circ/\text{h}$ 0 to 15 Hz $1.29^\circ/\text{h}$ 0 to 25 Hz	IUE, HEAO Production
Draper Labs/ Northrop	Third Gen. Gyro (TGG)	Magnetic suspension, gas spin bearing, single-degree-of-freedom, rate integrating gyro.	Classified	0.005 arc s 0.001 to 1 Hz 0.01 arc s 1 to 100 Hz	Production
Honeywell	GG-334	Single-degree-of-freedom, fluid floated, rate integrating gyro.	$0.017^\circ/\text{h}$	0.005 arc s 0.01 to 1 Hz 0.01 arc s 1 to 100 Hz	Unknown
Kearfott	Gyroflex	Two-degree-of-freedom, tuned rotor suspension	$0.01^\circ/\text{h}$	—	Production
	C 702519 (ATM)	Single-degree-of-freedom, fluid floated, rate integrating gyro.	$0.05^\circ/\text{h}$	—	Production Closed
Litton	G1200	Two-degree-of-freedom, tuned rotor suspension	$0.002^\circ/\text{h}$	—	Production
Northrop	GI-K7G	Single-degree-of-freedom, fluid floated, taut wire gimbal suspension, rate integrating gyro.	$0.010^\circ/\text{h}$	—	C5A Program Production Closed
Teledyne	SDG5	Two-degree-of-freedom, tuned rotor suspension	$0.001^\circ/\text{h}$	—	Limited Production
	SCAG	Two-degree-of-freedom, tuned rotor suspension	$0.001^\circ/\text{h}$	0 to 20 Hz < 1/20 arc s	Development

14  
ORIGINAL PAGE IS  
OF POOR QUALITY

ORIGINAL PAGE IS  
OF POOR QUALITY

TABLE IV-2. STAR TRACKERS

Manufacturer	Program	Field of View	Accuracy Uncalibrated	Accuracy with Fixed Calibration	Accuracy Calibrated	Noise Equivalent Angle	Time Constant	Minimum Visual Magnitude
Ball Brothers Research Corp.	SAS-C	$8^{\circ} \times 8^{\circ}$	$\pm 5$ arc min	1 arc min, $1 \sigma$	10 arc s, $1 \sigma$	5 arc s, rms	525 ms	6
	Shuttle	$10^{\circ} \times 10^{\circ}$			—	—	—	150 Brightest (S-20) Stars
Honeywell	HEAO-B	$2^{\circ} \times 2^{\circ}$	0.3 arc min	7.5 arc s ( $\pm 5^{\circ} \text{C}$ )	1.81 arc s	—	—	9

TABLE IV-3. SUN SENSORS

Manufacturer	Program/ Model	Type	Field of View	Resolution	Accuracy		Status
					Uncal.	Cal.	
Adcole	OAO/15381	Digital	64° × 64°	0.004°	0.017°		Flown
	IUE/18960	Digital	64° × 64°	0.004°	0.017°		Designed
	OAO/12202	Analog	30° Cone		1 arc min		Flown
	18980	Analog	70° Cone		2 arc min		New Design
	19770	Digital	±4°	0.22 arc s	5 arc s	1 arc s	Developmental
Ball Brothers Research Corp.	Solar Max	Analog	±2° to ±12° (Adjustable)	Linear Range	Null Accuracy		Flown Engineering Model Flown
	Wyoming SAM	Analog	±5°	±30 arc min	±5 arc s		
	SS-100	Analog	±15°	±30 arc min	±1 arc min		
	SS-200	Analog	±13°	±5°	±1 arc min		
	SS-1090	Analog	±15°	±20 arc min	15 arc s		
				±5°	2 arc min		
Honeywell	Skylab (ATM)	Analog	±2.5°	Resolution	Accuracy		Flown
				0.0625 arc s	2.25 arc s, 3σ		

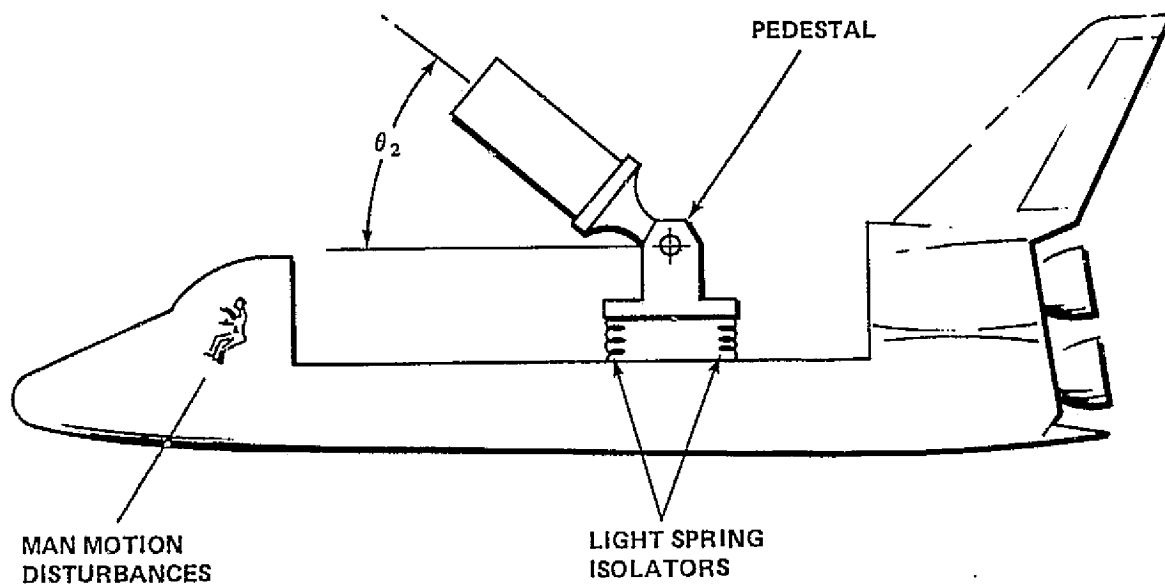


Figure V-1. Simulation model.

TABLE V-1. SUMMARY OF MASS CHARACTERISTICS

Item	Mass (kg)	Inertia (kg m <sup>2</sup> )
Shuttle/ Pallet	71 420	7 215 000
MPM Pedestal	23.4	2.34
Experiment Package		
Small	148	52
Large	500	500

TABLE V-2. SUMMARY OF MPM CHARACTERISTICS

Shock Mount Stiffness (N/m)		
Soft Mounted		100 and 250
Hard Mounted		$10^5$
Control Loop Bandwidth (Hz)		
Soft Mounted Inertial Pointing		3
Hard Mounted Inertial Pointing		0.5
Earth Surface Target Tracking		5

The system flow diagram shown in Figure V-2 depicts the dynamic interaction between the three bodies. The man motion disturbances on the Shuttle are partially attenuated by soft isolators. However, a most important function of the isolators to fine pointing is the freedom of the experiment to float relative to the Shuttle. The gimbal translates with the experiment while maintaining the desired pointing attitude.

Structural stiffness or gimbal compliance of the gimbal shaft was included between the pedestal and the experiment. The experiment control law has position plus rate feedback with the option of adding the integral of position feedback for tracking or slew maneuvers.

Crew motion was found to be the most significant disturbance during the Skylab missions. Since restraining crew motion is an unrealistic goal, the MPM should be designed to compensate for this activity. A design profile from Reference V-1 is shown in Figure V-3. A maximum force of 100 N was recommended to represent a typical level of crew activity within the Shuttle or Spacelab.

The dynamic model given in Appendix B was programmed on an analog computer. The analog computer was used to probe the overall system and determine control gains and isolator characteristics. A digital simulation was used to verify the analog results and to vary parameters that were inconvenient to vary in the analog simulation.

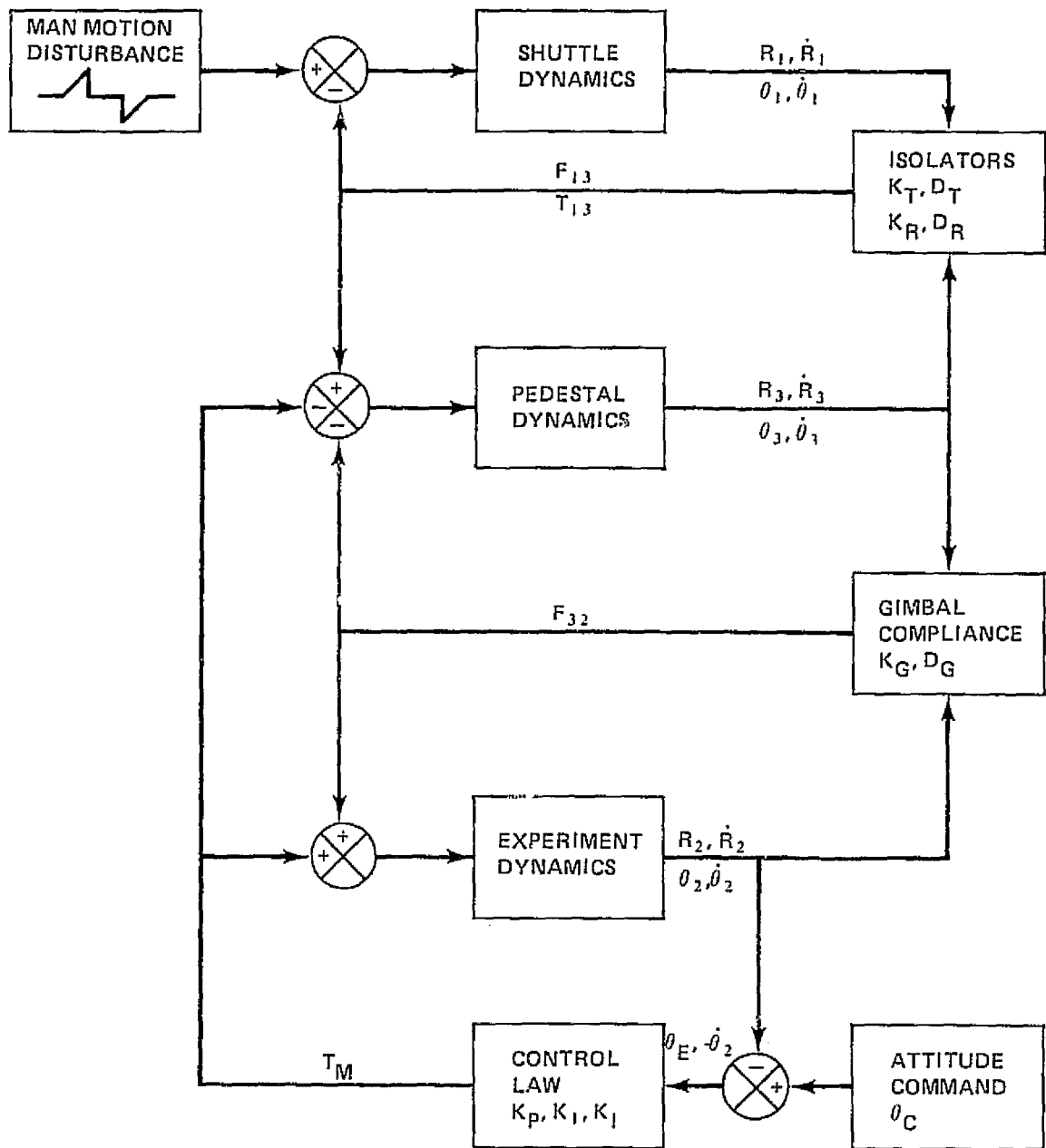


Figure V-2. System flow diagram.

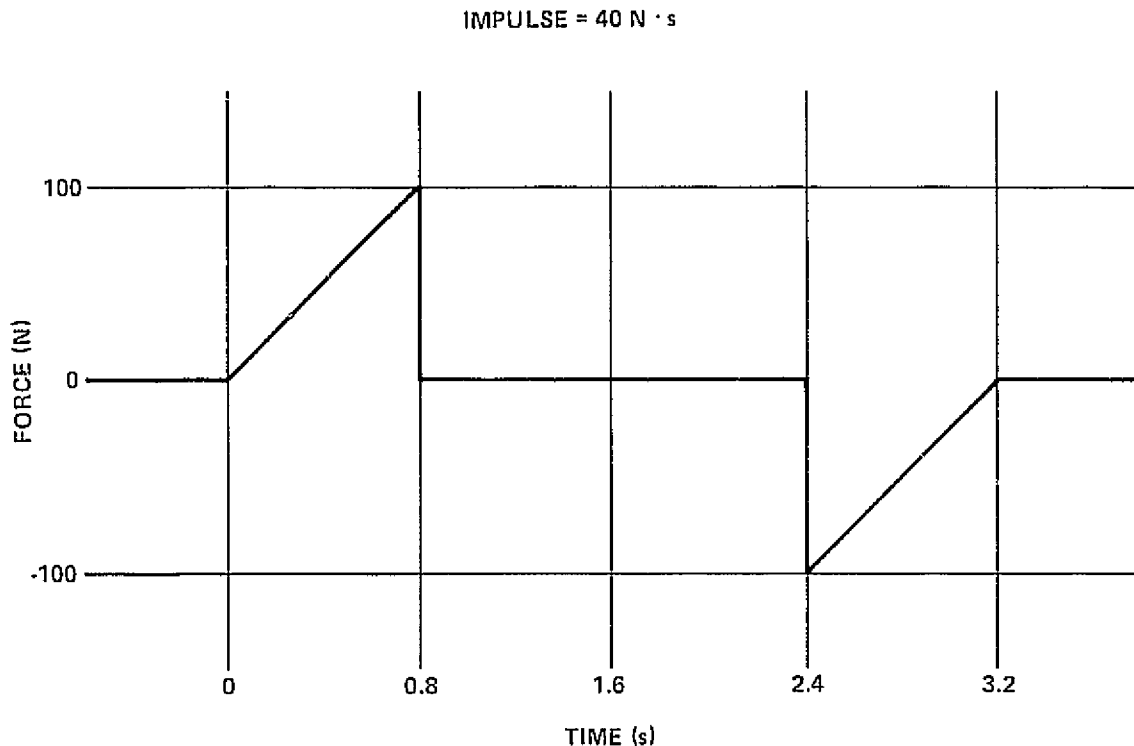


Figure V-3. Man motion design profile.

## VI. SIMULATION RESULTS

Stability, slewing, and tracking performance as well as control torque of the MPM were investigated using the planar simulation model. The computer output was in the form of chart recordings as a function of time for various system variables. Samples of these recordings are shown in Appendix C. The physical insight gained from observing the system dynamic response provided by the simulation is perhaps more important than the data. A computer simulation such as this one provides the only means for analyzing complex control problems because of the dynamic interaction of the system and the nature of the disturbing functions. It also provides a means for rapid assessment of alternate hardware proposals and pointing techniques.



The computer output has been processed for quick and easy interpretation and presented in Figures VI-1 through VI-3. Figures VI-1 and VI-2 show peak stability and control torque versus pointing position with Shuttle man motion disturbance of 30 kg and 500 kg instruments, respectively. The two bottom curves of each figure give both stability and control torque for soft shock mounts. The two soft mounted cases used shock mount stiffnesses of 100 N/m and 250 N/m, whereas in the hard mounted case the shock mount stiffness was  $10^5$  N/m. The soft shock mounts afford the fine pointing stability required by many scientific experiments. The hard mounted stability and control torque are also shown. The operating range for pointing position is  $40^\circ$  to  $90^\circ$ , which gives the best pointing stability and is within the present torque limit. The dynamic response plots corresponding to the summary charts in this section are located in Appendix C. Figure VI-3 shows the control torque exceeding the basic 0.6 N-m torque limit for a 500 kg instrument during the faster  $90^\circ$  slew maneuvers. However, the more important earth surface target tracking requirement is satisfied for altitudes above 300 km.

## VII. THERMAL CONTROL SYSTEMS

The thermal environment that will be seen by payloads on the Orbiter is different from that of most existing spacecraft. The Orbiter environment for all mission phases of launch, orbit, reentry, and post-landing and the constraints imposed by the Shuttle operations will need to be analyzed for each mission. Because of the very narrow temperature tolerances specified by the experiments, a passive system would be unsatisfactory. An active system using existing system technology and components was used where possible to keep development time and cost to a minimum. A fluid loop was selected with a shock mounted centrifugal pump to minimize vibration. A modular type radiator similar to the one used by the Orbiter was also selected. A thermal model was developed, and various orbital altitudes were examined.

This study was performed to conceptually design a thermal control system that will produce, in any orbit or vehicle orientation, a thermally controlled environment inside the canister to satisfy the requirements of the experiments.

Table VII-1 illustrates typical MPM instrument characteristics as determined from the "Shuttle Sortie Payload Description (SSPD)," dated July 1975. These data were used to determine some of the thermal control requirements.

PEAK STABILITY ERROR AND PEAK CONTROL TORQUE VERSUS POINTING POSITION FOR 130 kg INSTRUMENT (SCHWARZSCHILD) WITH SHUTTLE MAN MOTION DISTURBANCE  
 NO FRICTION OR CABLE TORQUE  
 NO SENSOR NOISE OR DRIFT

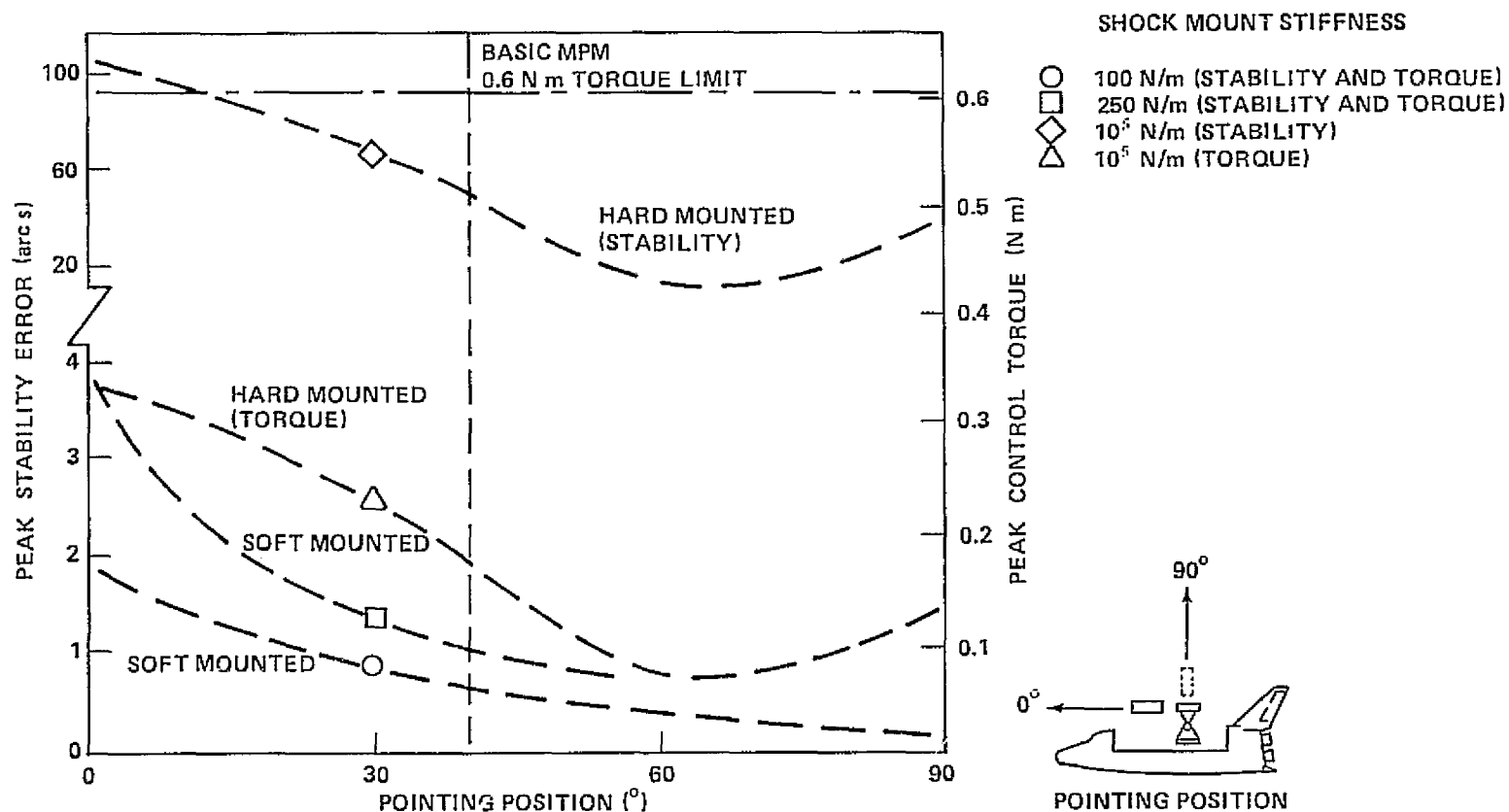


Figure VI-1. MPM pointing performance for 130 kg instrument.

PEAK STABILITY ERROR AND PEAK CONTROL TORQUE VERSUS POINTING POSITION FOR 500 kg INSTRUMENT WITH SHUTTLE MAN MOTION DISTURBANCE  
NO FRICTION OR CABLE TORQUES  
NO SENSOR NOISE OR DRIFT

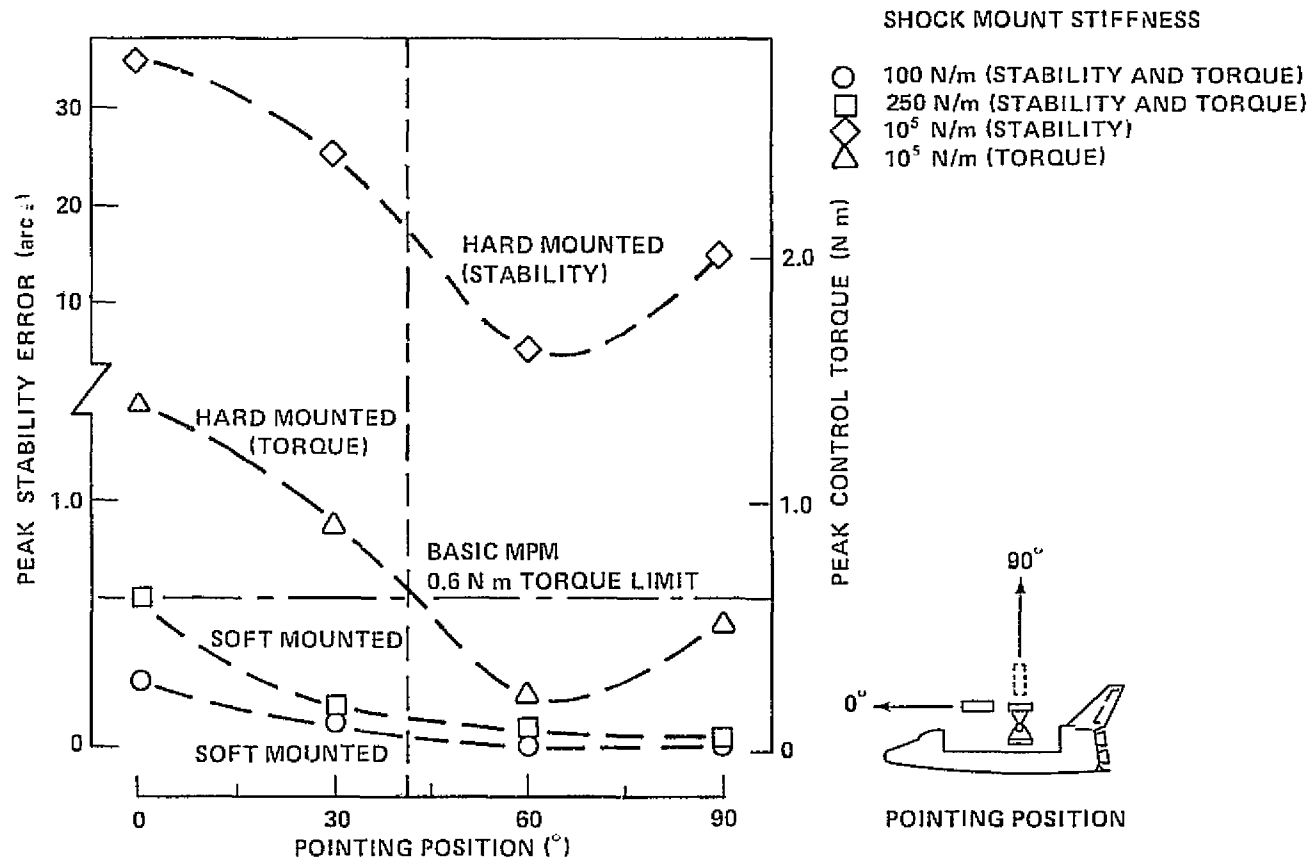


Figure VI-2. MPM pointing performance for 500 kg instrument.

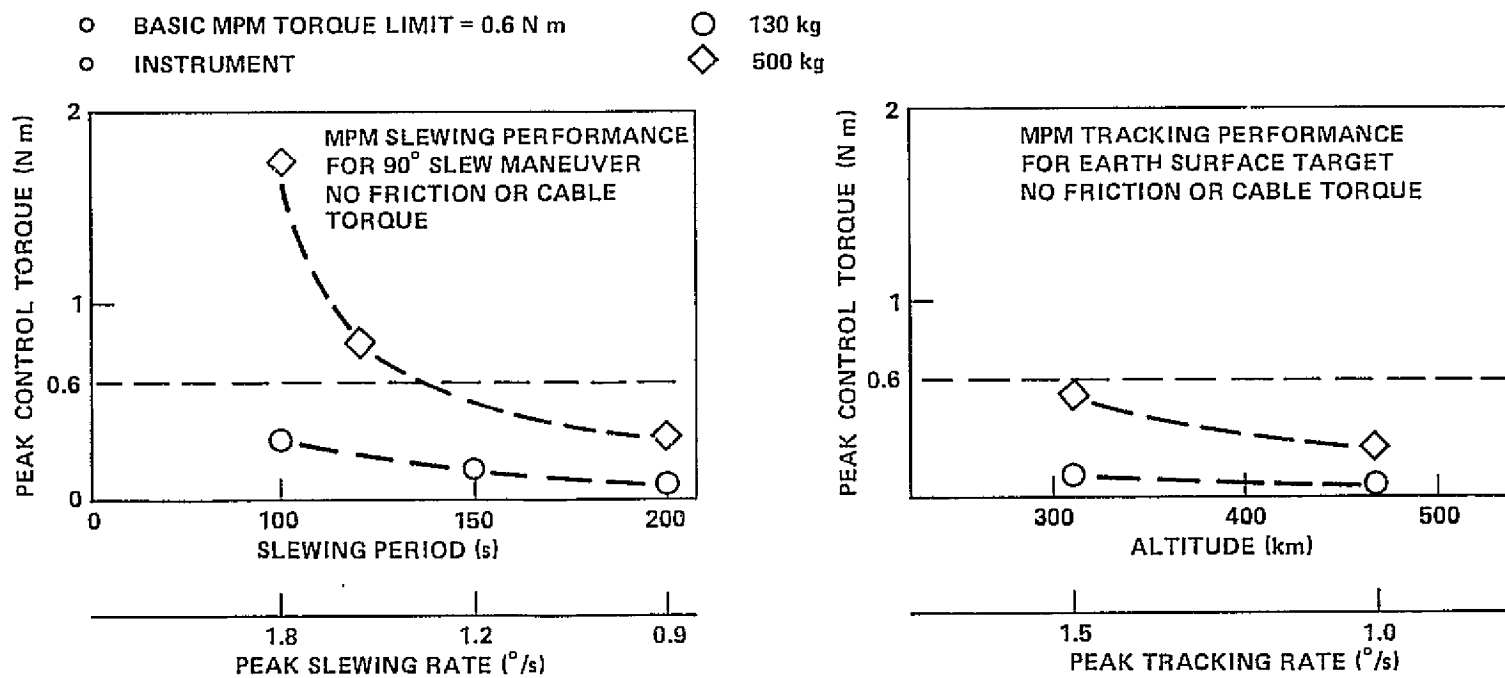


Figure VI-3. MPM slewing and tracking performance.

TABLE VII-1. MPM INSTRUMENT CHARACTERISTICS

	OPERATING TEMP (K)						LENGTH (m)				DIA (m)		OPER PWR (W)
	258	274	290	306	322	338	0	1	2	3	0	1	
AS-05-S	●		●				●				●		5
SO-05			●	●			●	●	●		●		15
SO-08			●	●			●	●	●		●		5
SCH CAM		●	●	●			●	●	●		●		80
H&I			●	●	●		●	●	●	●	●		153 MAX
SO-56		●	●	●			●	●	●		●		?
OP-76		●	●	●			●	●			●		190
OP-85			●	●	●		●	●			●		20
OP-86			●	●	●		●	●			●		18
OP-87			●	●	●		●	●			●		5
OP-88			●	●	●		●	●			●		15
OP-91		●	●	●	●		●	●			●	●	90
OP-78	●	●	●	●	●	●	●	●			●	●	200
OP-10		●	●	●	●		●	●			●		150
ST-025		●	●	●	●		●	●			●		100
ST-152		●	●	●	●		●	●			●		?
ST-ALL OTHER		●	●	●	●	●	●	●	MAX		●	MAX	60 MAX

Although the operating temperature covered a wide range, a 20°C temperature satisfied almost all instruments. Because of some very temperature sensitive instruments, a narrow temperature limit on the fluid loop was set to  $\pm 1^\circ\text{C}$ . A  $\pm 1^\circ\text{C}$  side-to-side and top-to-bottom temperature differential was selected. All instruments could be accommodated in a cylinder 1 m in diameter and 3 m long. The operating power ranged from 200 W to 5 W, which gave a heat load factor of 40 to 1.

Guidelines and assumptions utilized in this study are as follows:

- Circular orbit, 460 km
- Beta angle,  $52^\circ$
- Payload bay orientations
  - Solar oriented
  - Earth oriented
  - Line normal to payload bay,  $30^\circ$  off solar vector
  - Line normal to payload bay,  $90^\circ$  off solar vector
- Surface optical properties  $\alpha/\epsilon$ 

—Radiator	0.08/0.8
—Canister body	0.35/0.8
—Pallet surface	0.27/0.9
—Spacelab	0.27/0.9
—Shuttle radiators	0.08/0.8
—Cargo bay	0.2/0.5
- Maximum heat load, 200 W

A fluid loop system with the radiator mounted concentrically on the forward end of the canister was selected as the method of thermal control. Figures VII-1 and VII-2 present the configuration and the system schematic. The basic philosophy was that all the heat dissipated in the canister must be picked up by the fluids and dumped by the radiator. To provide the tolerances required, the variations of the external environment must be completely isolated from the inside wall. Therefore, a minimum of 5 cm of aluminized Mylar insulation is required over the canister. For meteoroid protection and structural integrity, the radiator tubes are covered by a 0.3 mm aluminum sheet. To provide temperature uniformity inside the canister, the inlet line distributes coolant evenly

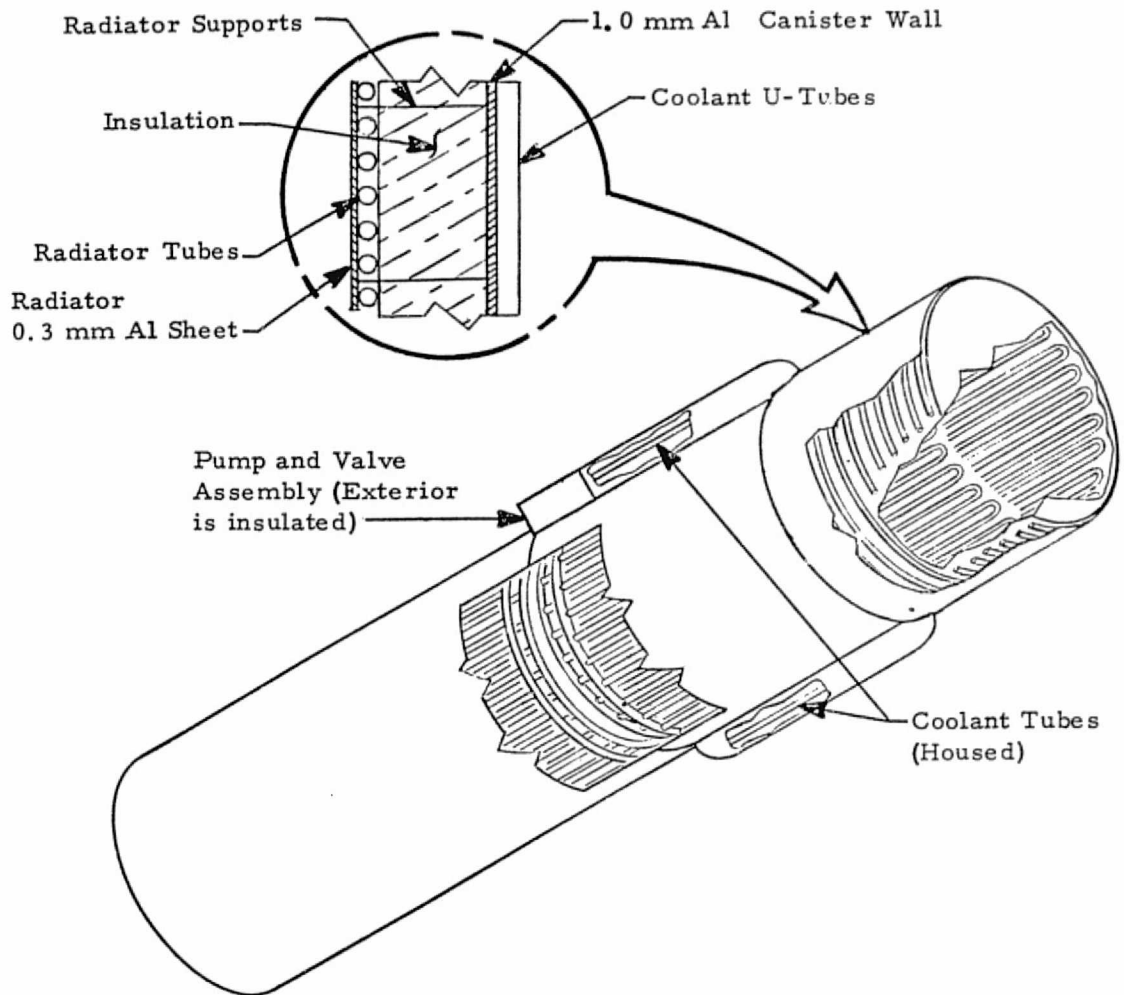


Figure VII-1. MPM thermal control concept.

around the periphery by means of a concentric manifold and closely spaced U-tubes. The inside tubes and wall must have a high emissive surface to provide the maximum radiation interchange. The coolant makes one pass to the end of the canister and back to an outlet concentric manifold. Since the canister structural design is such that it can be separated at the midpoint and only the top half used to house smaller experiments, the thermal control system must be able to accommodate this requirement. This is accomplished by mounting the pump and radiator connecting lines on the canister half that contains the radiator and by

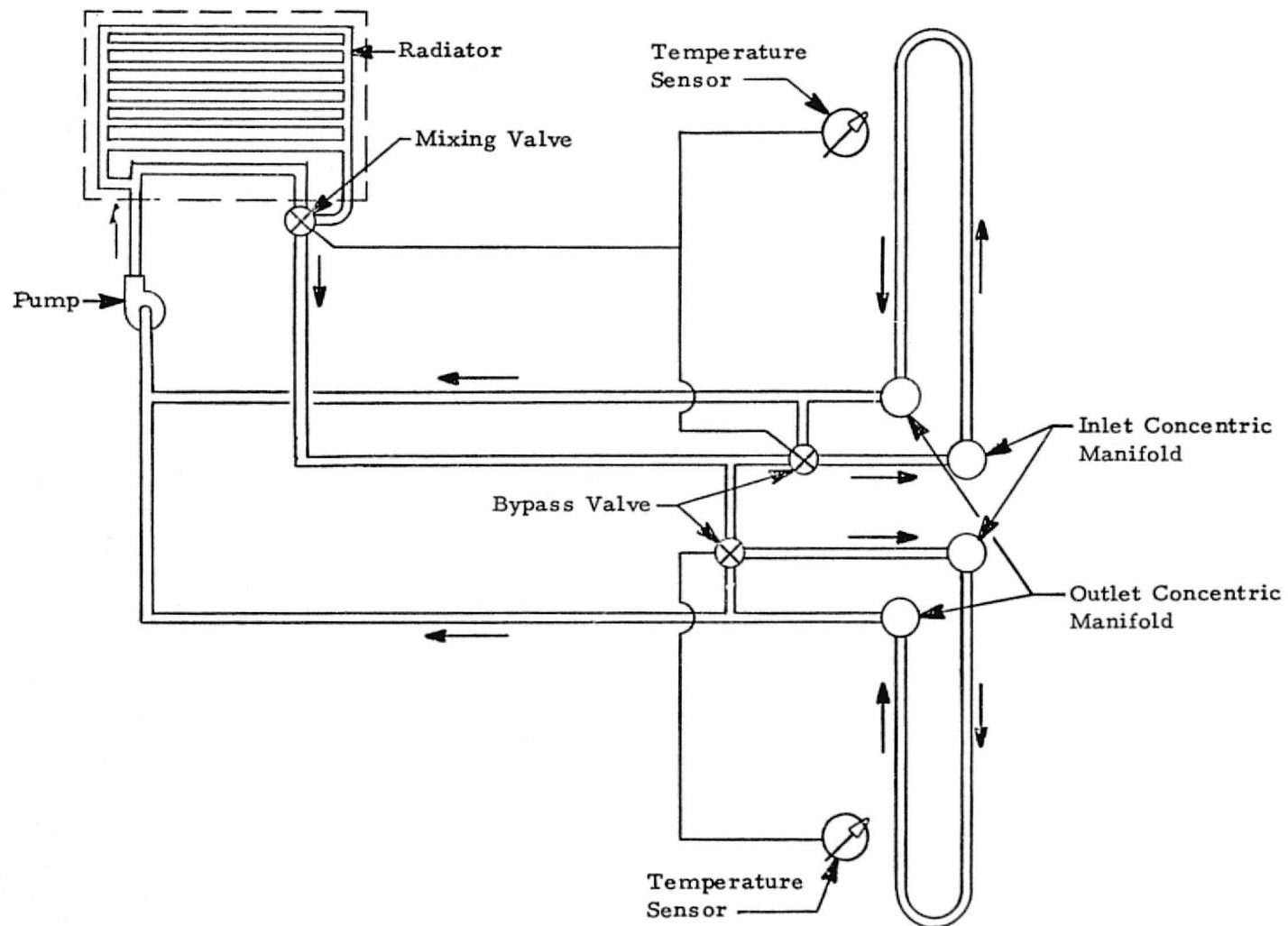


Figure VII-2. MPM thermal control schematic.



means of quick disconnects and flex lines connected to a duplicate manifold system (as described previously) for the bottom half. Feedback temperature sensors on the inside wall regulate the mixing and bypass valves to provide the coolant flow required to keep the inside environment within the specified tolerance.

A thermal model, with the MPM canister relatively located within the payload bay as shown in Figure VII-3, was constructed to determine a feasible radiator size that would keep the system within reasonable weight and power limits. A 1.5 m length representing the shortened canister was used because it has a smaller view factor to space, thereby making it a worst case. Four cases were analyzed with a radiator area of  $1.92 \text{ m}^2$  and an applied heat load of 200 W. These were:

- Payload bay normal aligned with solar vector
- Payload bay normal aligned with local vertical
- Payload bay normal  $30^\circ$  off solar vector with canister aligned with solar vector
- Payload bay normal  $90^\circ$  off solar vector

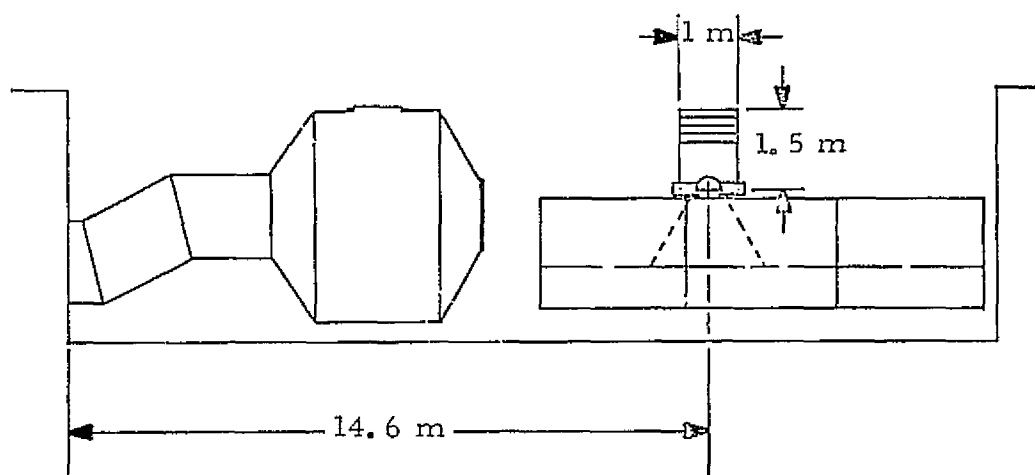


Figure VII-3. Thermal model relative mounting position.

Resulting temperatures are presented in Figures VII-4 through VII-7. The important temperature is that of the radiator and the difference between it and the limits required by the canister. A minimum temperature difference ( $\Delta T$ ) of  $10^{\circ}\text{C}$  is desired to keep the power and pump weight at a reasonable level. For these cases the minimum  $\Delta T$  was  $20^{\circ}\text{C}$ , which is well above the desired level. There was an insignificant difference in the radiator temperature of the first three cases. A somewhat colder temperature resulted from the case with the payload bay facing  $90^{\circ}$  to the solar vector. The solar-oriented case was rerun with a  $0.96\text{ m}^2$  radiator area incorporated. The results are presented in Figure VII-8. As can be seen, this surface area is inadequate because the radiator temperature exceeded the canister limits during part of the orbit. Figure VII-9 shows the maximum surface temperature of the canister during and after reentry.

It is assumed for this study that over a small temperature range, the temperature varies linearly as a function of radiator area. Based on this assumption, a plot of temperature difference between the radiator and inside wall limits as a function of radiator area is presented in Figure VII-10. Also presented in this figure are approximate curves of pumping power and pump weight as a function of the temperature difference. These curves are based on calculations utilizing 13 mm diameter tubing and the coolant properties of fluorochemical liquid (FC-75), which are:

- Density —  $1.76\text{ gm/cm}^3$
- Dynamic viscosity at  $20^{\circ}\text{C}$  —  $1.488\text{ mPa}$
- Boiling point at 1 atm —  $101^{\circ}\text{C}$
- Freezing point —  $-113^{\circ}\text{C}$
- Vapor pressure at  $20^{\circ}\text{C}$  —  $3.45\text{ kPa}$

Two pumps were selected as baseline candidates for the present study. The first uses one Hydroair 68-3170 gear pump having the following characteristics:

- Capacity —  $3.2\text{ cm}^3/\text{s}$
- Power —  $30\text{ W}$
- Weight —  $1\text{ kg}$
- Minimum Life —  $2000\text{ h}$

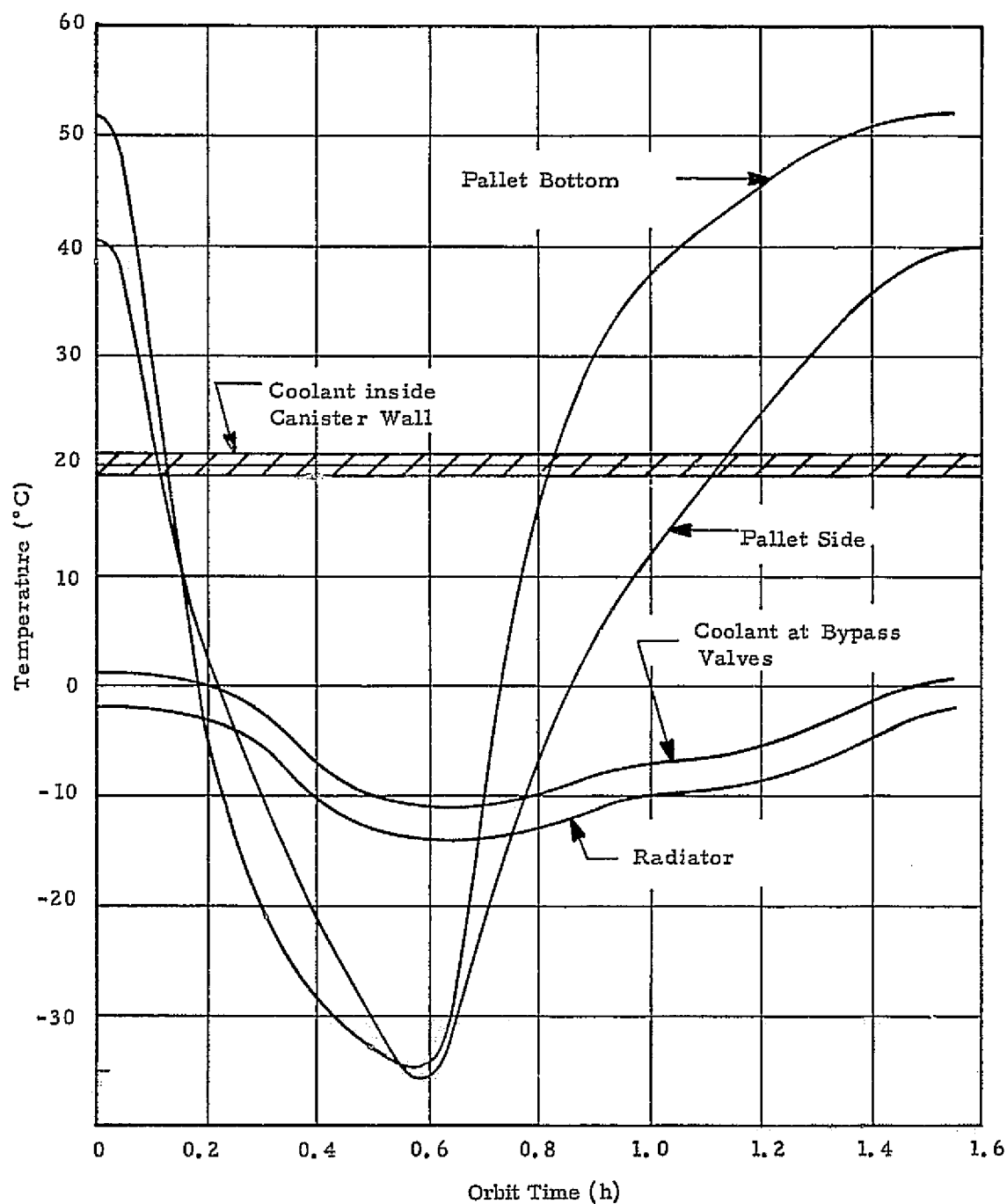


Figure VII-4. Significant temperatures on thermal model with payload bay and MPM canister solar oriented (radiator area is  $1.92 \text{ m}^2$ ).

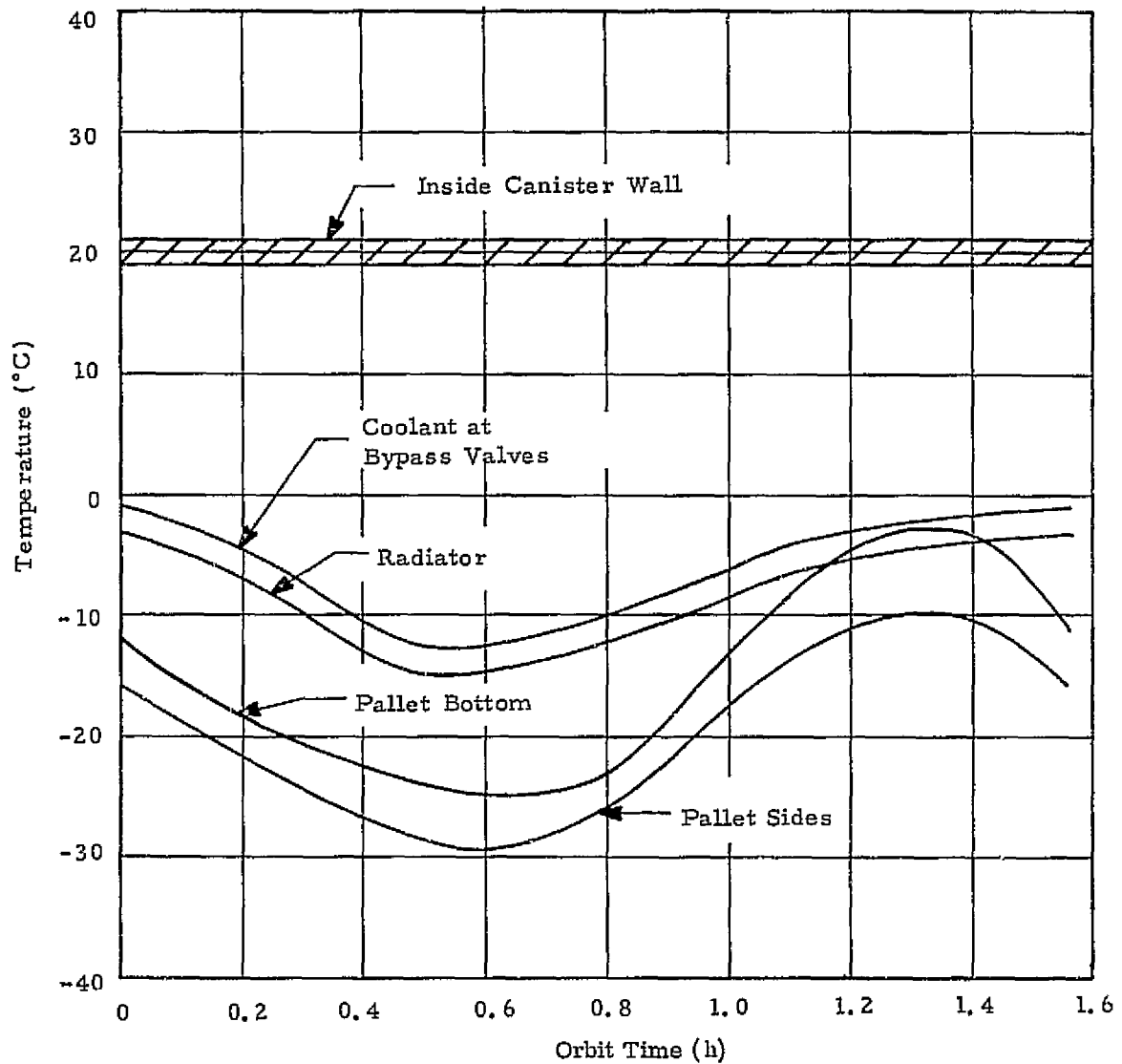


Figure VII-5. Significant temperatures on thermal model with payload bay and MPM canister pointed to the local vertical (radiator area is  $1.92 \text{ m}^2$ ).

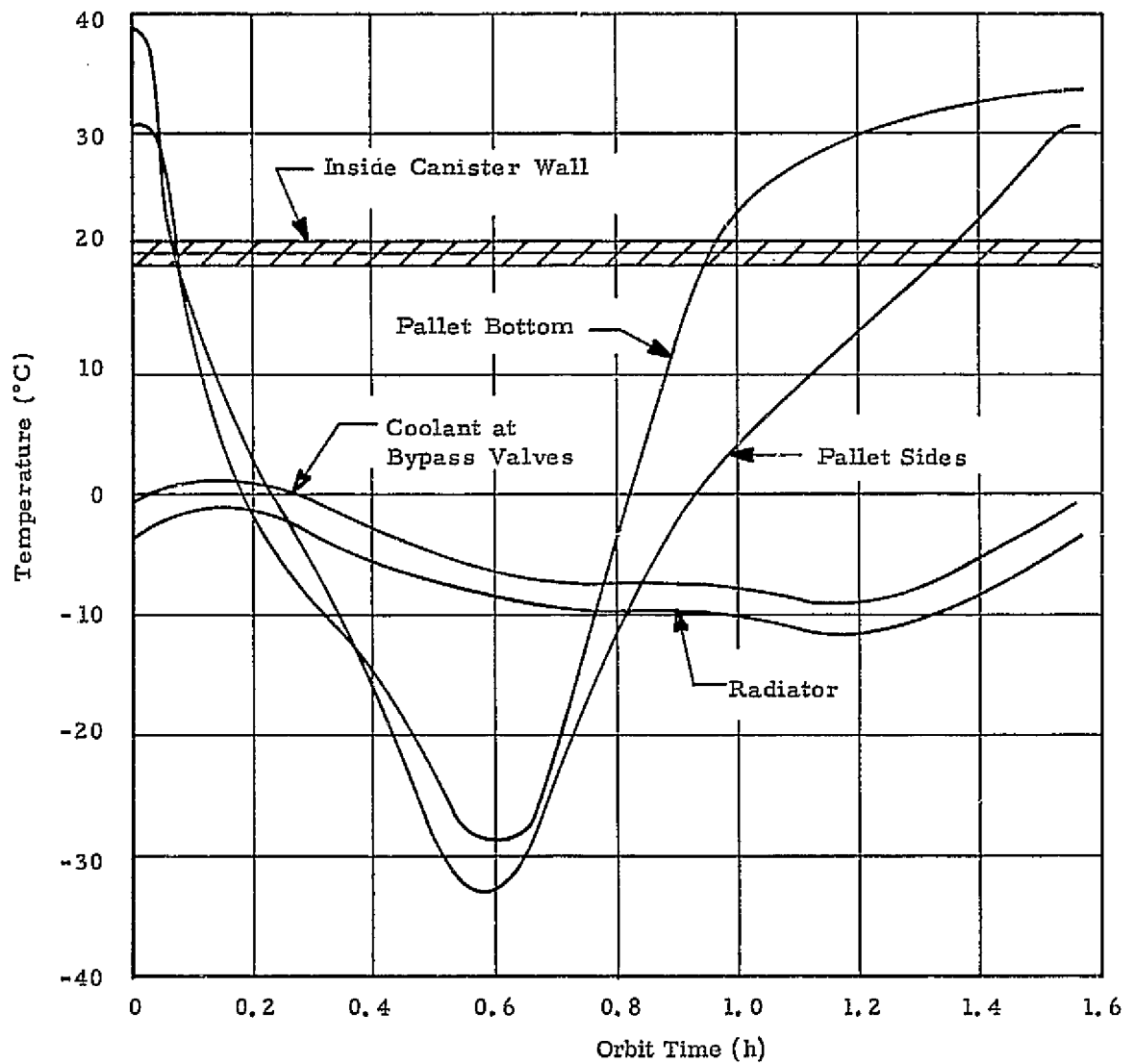


Figure VII-6. Significant temperatures on thermal model with payload bay normal axis oriented  $30^\circ$  off the solar vector and MPM pointed toward the sun (radiator area is  $1.92 \text{ m}^2$ ).

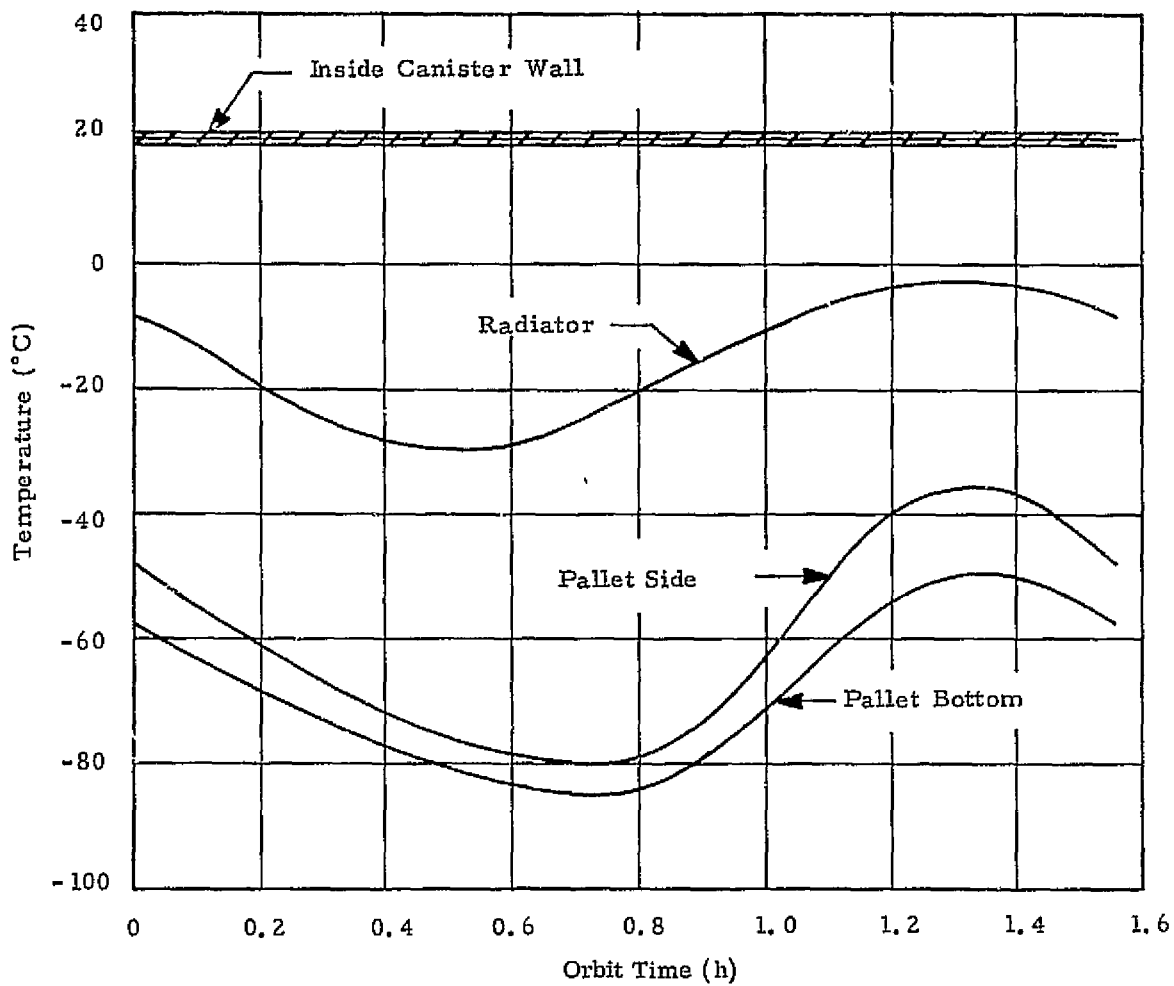


Figure VII-7. Significant temperatures on thermal model with payload bay and MPM canister facing  $90^\circ$  from solar vector (radiator area is  $1.92 \text{ m}^2$ ).

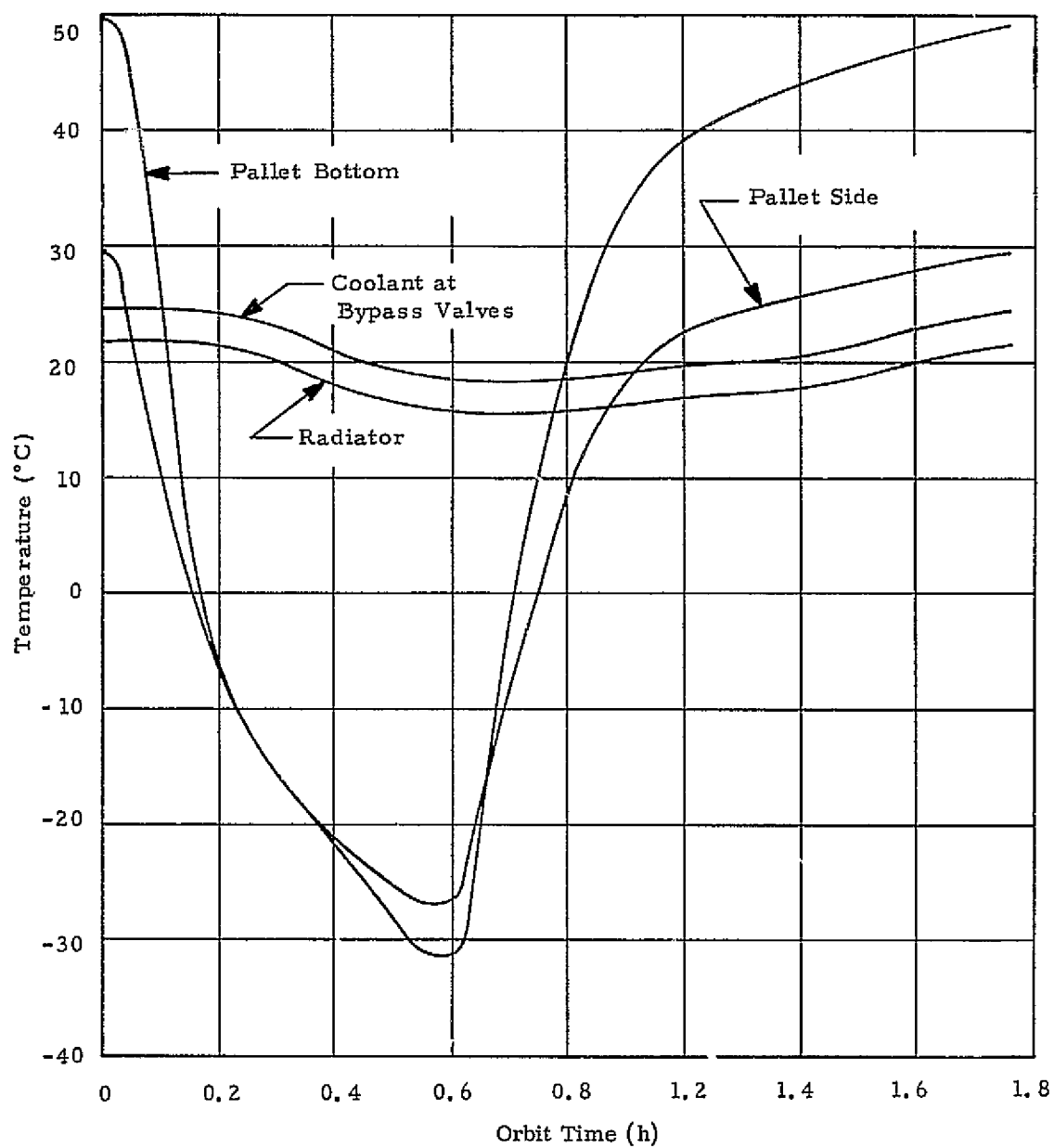


Figure VII-8. Significant temperatures on thermal model with payload bay and MPM canister oriented toward the sun (radiator area is  $0.92 \text{ m}^2$ ).

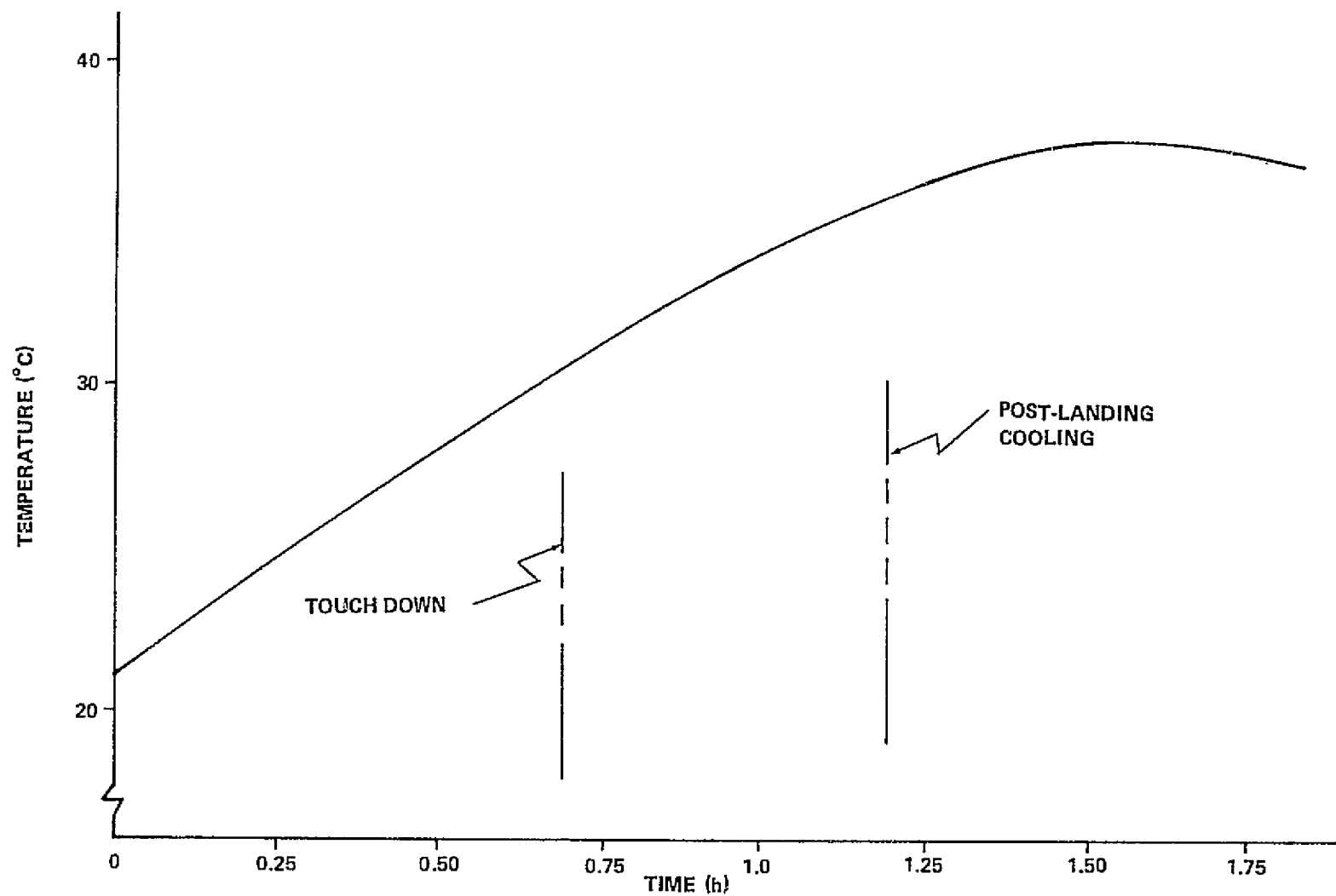


Figure VII-9. Typical entry profile.



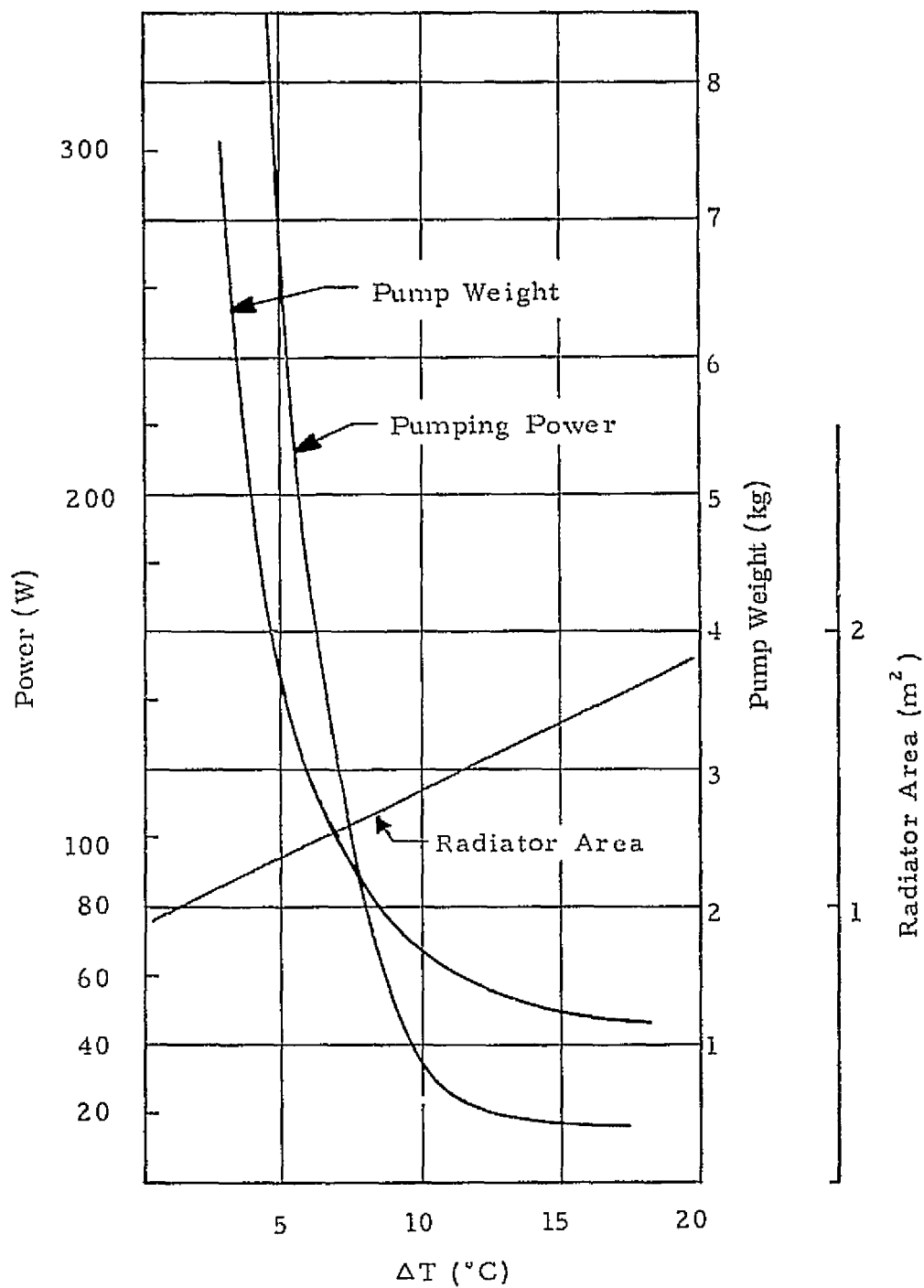


Figure VII-10. Pump power, weight, and radiator area as a function of temperature difference between radiator and inside wall limits.

The second uses three centrifugal Dray Hydroair 60-659 pumps having the following characteristics:

- Capacity —  $1.2 \text{ cm}^3/\text{s}$
- Power — 5.6 W
- Weight — 0.27 kg
- Minimum Life — 2000 h

Because of the inherent lower vibration in the centrifugal pump, it was chosen for this study. Three pumps will give a higher reliability; if one should fail, the remaining two will provide some cooling capacity.

The weight of the overall MPM thermal control system is summarized in Table VII-2.

TABLE VII-2. MPM THERMAL CONTROL  
SYSTEM WEIGHT

Structure	50 kg
Radiator	10 kg
Paint	10 kg
Pump	2 kg
Insulation	12 kg
Plumbing	4 kg
Contingency	9
Total	97 kg

## VIII. PRELAUNCH TEST AND VERIFICATION PHILOSOPHY

The light spring isolators that are used for the ESA IPS and the MPM will not support the mass of the mount in an earth gravity environment. Any test fixture that is used to provide additional support will almost certainly alter the isolator characteristics to a significant extent. The offset mass of the payload from the gimbal axes will create loads in excess of torquer capabilities for angles more than a few degrees from the gravity vector. However, the mass offset problem can be essentially overcome by counter balancing, special test fixtures, or restricting gimbal angles.

These two problems add to the heavy burden of ground testing precision pointing equipment for space application. Functional testing of either the spring isolator or conventional concepts does not present any significant problems. However, verification of arc-second performance under a simulated space environment is practically impossible for either concept. Conventional concepts must cope with the offset mass that results from balancing uncertainty, deformation of structure in a 1 gravity field, and additional bearing loads. Earth rotation and gravity introduce errors into inertial sensors which must be removed or compensated for in the simulation. Optical sensors must be provided with a source that accurately represents the sun or star. High fidelity sources that can provide a sub-arc-second reference are either very expensive or nonexistent. The atmosphere usually prohibits the use of natural sources. Other problems are isolation from air currents and disturbances transmitted through the ground.

Ground testing of the ATM Experiment Pointing Control System (EPCS) was performed in a specially designed facility resting on a solid concrete block that was 6.4 m (21 ft) wide, 5.2 m (17 ft) deep, and 12.2 m (40 ft) long. The mass of the experiment was supported in a mercury pool. The facility was designed to minimize reflected light and convection currents of the air. State-of-the-art star and sun sources were employed. Laser interferometers were used to measure experiment stability. The development of this facility and performance testing of the ATM EPCS required about 5 years.

The specified performance level for the ATM EPCS was  $\pm 2.5$  arc s about the line of sight. Ground testing did not verify performance beyond approximately  $\pm 10$  arc s. Actual orbital performance was found to be about  $\pm 1$  arc s.

Based on this experience, performance testing of precision pointing equipment in a gravity environment appears to be expensive, inadequate, and not absolutely necessary to assure high accuracy in orbit. This argument is especially applicable to Shuttle flights that should provide the means for verification testing in an orbital environment.

## IX. CONCLUSIONS AND RECOMMENDATIONS

The light spring isolator concept provides an effective and economical means of disturbance isolation and does not restrict gimbal location or experiment center of mass. This concept can be applied to existing ATM hardware to create high performance pointing mounts at minimum cost. Development should begin in the near future on hardware modifications that would result in small instrument mounts that would supplement the Spacelab IPS.

Simulation results indicate that the MPM can capture a large percentage of Spacelab experiments. Stability levels of  $\pm 1$  arc s or better can be maintained during reasonable crew motion and thruster operation. More detailed simulations should be performed on this concept as soon as better hardware characteristics, such as experiment flexibility, are known.

The thermal design concept developed for the MPM is a proven design. Using the new wide heat dissipation range space radiator developed for the Orbiter and other existing off-the-shelf hardware will keep cost to a minimum. The fluid loop is a reliable and versatile system capable of multiple missions and a wide range of environmental characteristics. Heat pipes could be employed to accomplish the same temperature limits but because of developmental engineering and testing, the cost would be too great.

The thermal canister affords a versatile tool that will house many different payloads. It is light in weight, and testing will not have to be accomplished from one payload to another.

The MPM provides an efficient means of pointing small payloads and can serve as a precursor to the Spacelab IPS. The autonomy of this design makes it especially applicable to early Shuttle flights. The use of available ATM hardware for all major elements keeps both development and unit costs to an absolute minimum. The MPM is the obvious solution to many Spacelab pointing problems.

## APPENDIX A

### STAR TRACKER FOR THE APOLLO TELESCOPE MOUNT

#### Introduction

The ATM Star Tracker provided coordinate information to establish roll information for the Skylab vehicle. It consists of two assemblies, the optical mechanical assembly (OMA) and the Star Tracker electronics (STE). Gimbal drive electronics and power supplies are also included in the STE.

The OMA (Fig. A-1) consists of a Star Tracker assembly mounted on a double gimbal suspension. Inner and outer gimbal pivots contain a torquer-tachometer assembly and an encoder assembly. The complete gimbal assembly is supported with a three-point mounting frame.

#### Specifications

Specifications for the system are as follows:

	<u>Weight (kg)</u>	<u>Size (m)</u>	<u>Power Dissipated (W)</u>
OMA	18	$0.43 \times 0.32 \times 0.53$	30.36 (max.) 8.6 (avg.) 20 (heaters)
STE	10	$0.47 \times 0.29 \times 0.16$	18.7 (max.) 15.1 (avg.)

Gimbal Freedom: Outer  $\pm 1.51$  rad; inner  $\pm 0.70$  rad

Gimbal Readout: Digital — serial binary to ATM digital computer;  
parallel binary to telemetry

Gimbal Position Resolution:  $145 \mu\text{rad}$  (for ATM digital computer  
and telemetry)  
 $290 \mu\text{rad}$  (for ATM control and  
display)

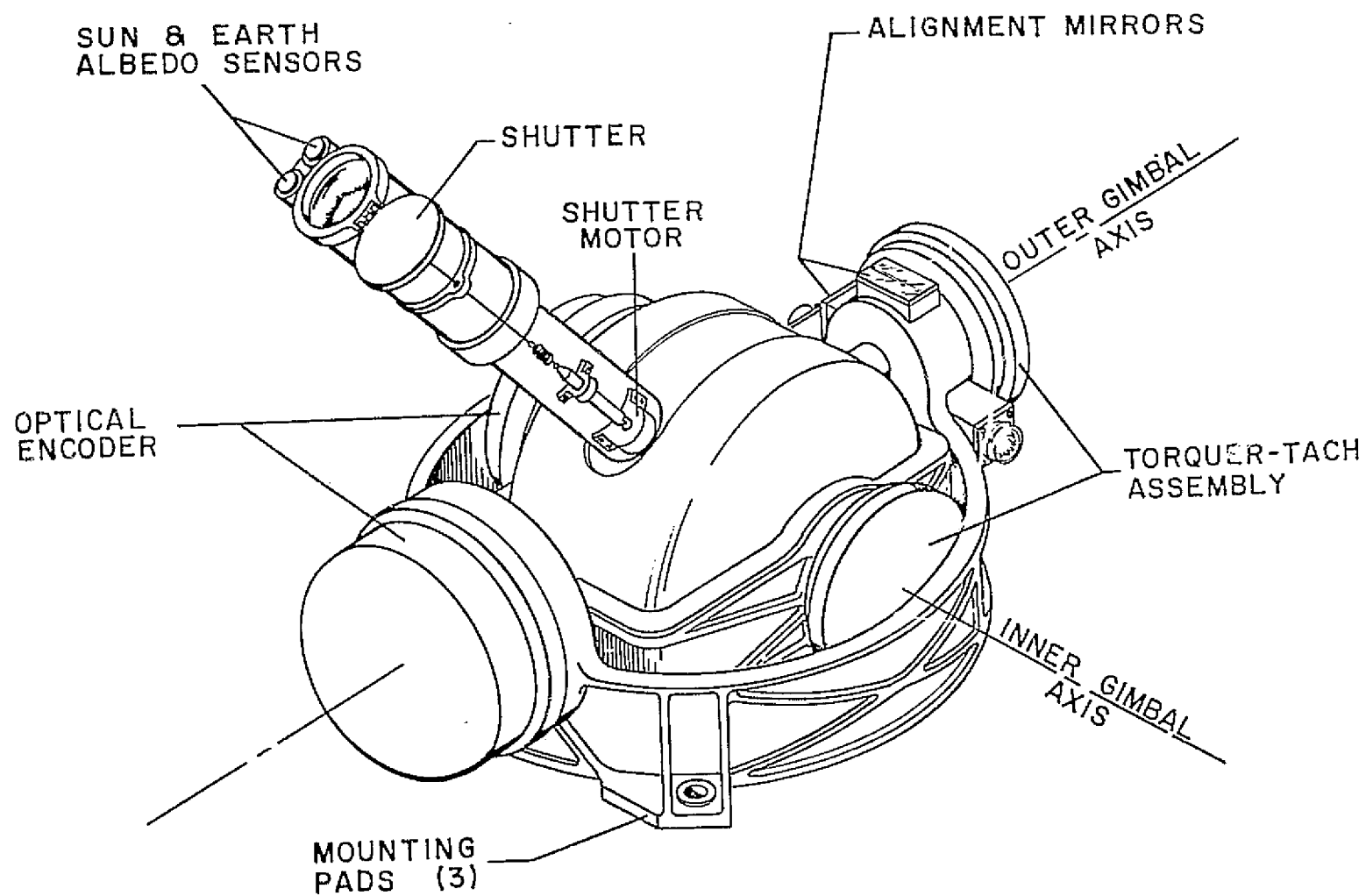


Figure A-1. Star tracker optical-mechanical assembly.

Gimbal Position Accuracy:  $\pm 145 \mu\text{rad}$ ,  $1\sigma$

Gimbal Torque: 0.64 N-m (max.)

Modes of Operation: Manual (from hand controller), automatic,  
or shutter close/hold

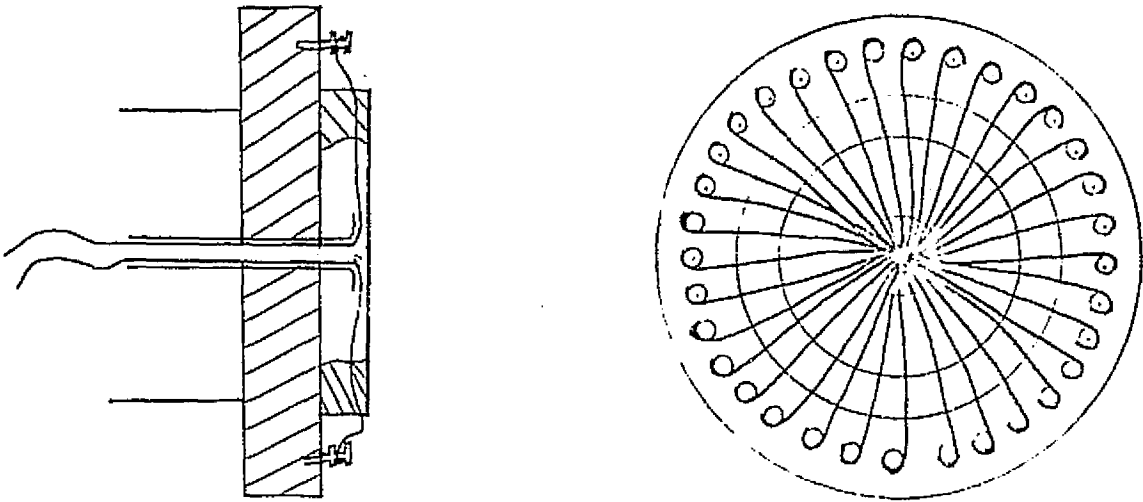
## Mechanical Description

The star tracker OMA comprises a refractive telescope mounted in a double gimbal suspension. Gimbal freedom is  $\pm 1.51$  rad around the outer gimbal axis and  $\pm 0.70$  rad around the inner gimbal axis. Major elements in the mechanical assembly consist of the frame, gimbal, inner and outer torquer pivots, inner and outer encoder pivots, and the telescope assembly which also includes the sunshade and shutter.

To afford maximum gimbal rigidity and avoid sliding fit hangup, both bearing pairs in both gimbal pivots are securely preloaded. This requires a close match of material coefficients. To provide a lightweight alloy with a coefficient of expansion matching stainless steel, A-390 aluminum alloy is used for the frame and gimbals. A three-point mount below the center of gravity is located on the frame. The frame pivot bores are line-bored accurately with respect to the plane of the mounting feet and also the pad which receives an alignment reference mirror.

The gimbal torquer pivots consist of a housing, shaft, bearings, torque motor, rate tachometer, flex leads, terminal board, and cover. Basically, a pair of 440C, preloaded, angular contact ball bearings accurately pivots the shaft on which the motor and tachometer rotor adapters are mounted. To ensure interchangeability, each assembly is constructed such that a close tolerance dimension is held between the locating flanges on the housing and the shaft. The flex leads (Fig. A-2) consist of 53 number 30 AWG and 29 number 30 AWG wires on the outer and inner pivots, respectively.

The gimbal encoder pivots consist of essentially the same parts as the torquer pivots, except the torque motor and rate tachometer are replaced by an encoder assembly. This assembly consists of a hub, mounting plate, angular contact bearing pair, coded optical disk, light source, readout array, and a pair of printed circuit component boards. Rotational coupling between the pivot shaft and the encoder disk hub is by means of a metal bellows.



NUMBER OF WIRES PER PIVOT (PRESENT CONFIGURATION)

OUTER PIVOT – 53 NO. 30 AWG

INNER PIVOT – 29 NO. 30 AWG

Figure A-2. Flex lead configuration.

To provide long term reliable lubrication with the smooth performance required, a system employing a fluorosilicone oil is used.

To permit tracking a guide star within  $0.78$  rad of the sun line and  $8.7 \times 10^{-2}$  rad of earth reflection, a sunshade is extended beyond the lens along the optical axis. The assembly consists of a machined aluminum tube with black optical baffles. A sun sensor and earth sensor are mounted adjacent to the open entry of the tube. A hinged shutter door provides closure of the tube against contamination and damaging high-intensity stray light. The shutter is spring-loaded to open, and a steel tape is wrapped around a drum to return the door to a closed position as required. Pull force is exerted on the tape by means of a jackscrew and a nut driven by a dc torquer motor. (Note: The Star Tracker and sunshade will be removed for the MPM.)



## Thermal Design and Requirements

Sink temperatures of the star tracker OMA have been calculated to be  $-84.4^{\circ}\text{C}$  nonoperating and  $-56.7^{\circ}\text{C}$  operating on the ATM. The OMA design has considered these environmental conditions as well as the temperature limits of the components.

Heaters have been provided on the OMA to maintain a minimum temperature of  $-18^{\circ}\text{C}$ . The heaters are located as follows: telescope housing, 10 W; gimbal-mounted encoder, 10 W; and frame-mounted encoder, 10 W. Twin power resistors are located on the encoder pivots and a tube type heater is located in the telescope housing. Disk type thermostat switches directly control the heaters and are arranged in a series-parallel circuit for more reliability.

Inner and outer encoder covers are insulated with a fiberglass liner and multilayer aluminized Mylar sandwich material. The outer frame is provided with a lower cover to reduce heat rejection toward the vehicle rack. This cover is formed of heat-treated 0.031 aluminum alloy, the OMA side being fitted with an aluminized multilayer Mylar blanket. The lower side is painted with Pyromark white paint. Fiberglass spacers are used at points of attachment to the frame flange. The inside surfaces of the OMA are painted with Cat-A-Lac epoxy black paint. External surfaces are painted with Pyromark white. The STE is painted with Cat-A-Lac black also.

An adiabatic interface is to be provided between the OMA mounting bracket and the rack structure. The mounting bracket will be insulated with the OMA frame to maintain the bracket at the same thermal level as the Star Tracker. The mounting bracket also will be made of stainless steel with a matching coefficient of expansion of A-390 to assure a minimum stress. These design requirements will prevent excessive mechanical stresses in the Star Tracker gimbals from temperature gradients.

## Servo Electronics

The gimbal servo system consists of a rate-controlled driver that varies the gimbal position and/or rate according to commands from a number of different sources. The two gimbals and their functions are similar, so only one will be described here. Figure A-3 is a block diagram of the essential elements of the system.

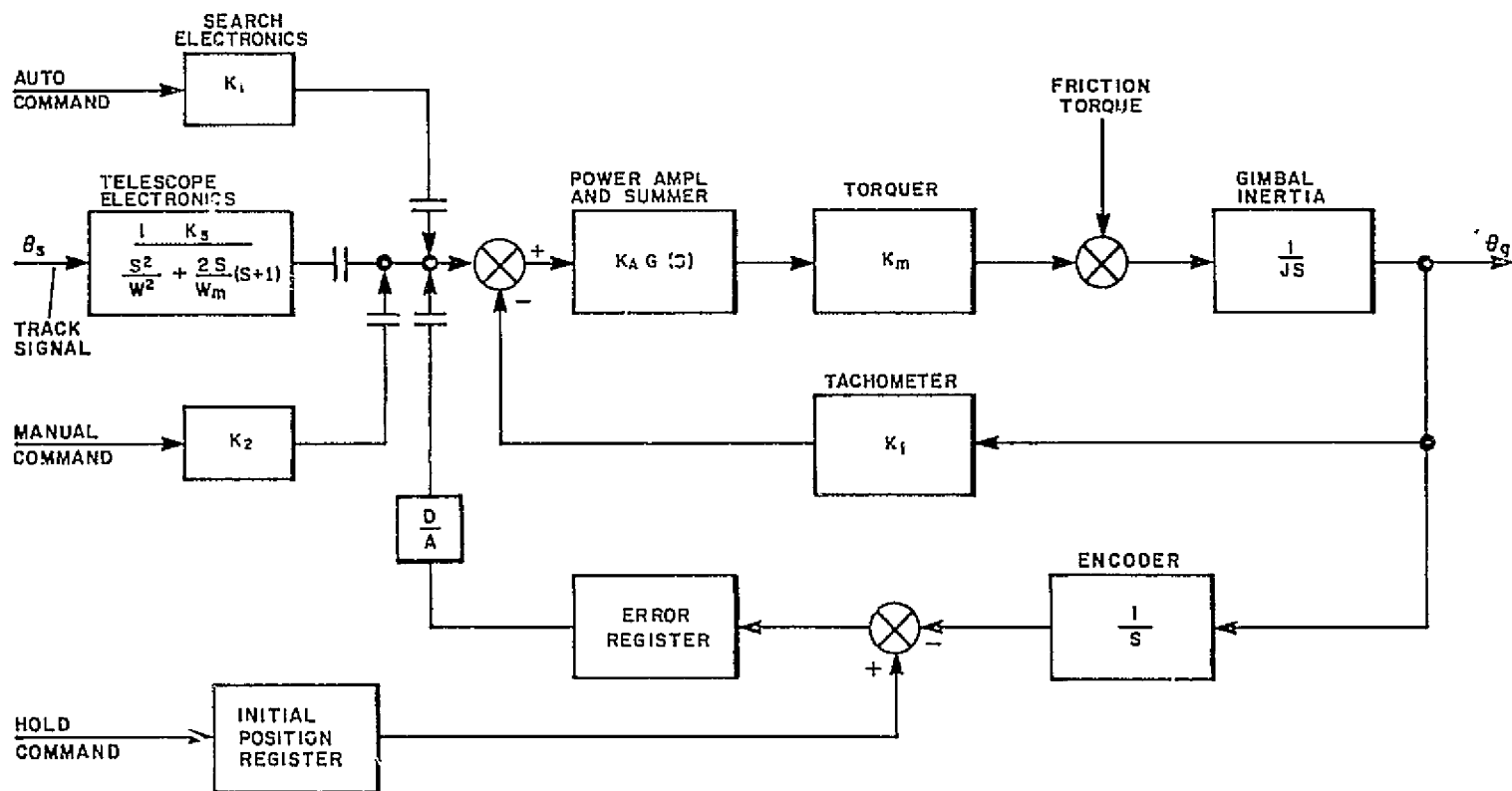


Figure A-3. Block diagram of ATM Star Tracker gimbal servo system.

There are four different modes of operation; hence, there are four inputs to the rate loop electronics (Fig. A-3). The power amplifier and summing network constitute the entire electronics, and these electronics are compensated to accommodate both the telescope loop and the encoder position loop. The torquer (an Inland model 2201) drives the gimbal inertia and friction and produces a rate. This rate is measured by a tachometer (Inland model TG 2123) and fed back to force the gimbal to move at a constant rate determined by the command input. This rate is also kinematically integrated to produce position information that is measured by an optical encoder. In the hold mode, the position difference signal will be fed back to become the rate command input and bring this error to zero.

## APPENDIX B

### DYNAMIC MODEL

The equations of motion were developed for a three-body planar model as depicted in Figure B-1. The three bodies were a Shuttle with pallet, a pedestal with isolators, and a base plate with experiment. All motion was restricted to a plane resulting in two degrees-of-freedom in translation and one degree-of-freedom in rotation for each of the bodies. The coordinate directions are shown for each of the three bodies and an inertial coordinate (G) in Figure B-1.

The translational equations of the three bodies are as follows:

$$M_1 \ddot{R}_{1X} = F_{1X} - \theta_1 F_{1Z} - F_{13X} \quad (B-1)$$

$$M_1 \ddot{R}_{1Z} = F_{1Z} + \theta_1 F_{1X} - F_{13Z} \quad (B-2)$$

$$M_2 \ddot{R}_{2X} = F_{32X} \quad (B-3)$$

$$M_2 \ddot{R}_{2Z} = F_{32Z} \quad (B-4)$$

$$M_3 \ddot{R}_{3X} = F_{13X} - F_{32X} \quad (B-5)$$

$$M_3 \ddot{R}_{3Z} = F_{13Z} - F_{32Z} \quad , \quad (B-6)$$

where

$$\begin{aligned} F_{13X} = & K_{TX} (R_{1X} + RH1_X + \theta_1 RH1_Z - R_{3X} - RS_X - \theta_3 RS_Z) \\ & - D_{TX} [R_{3X} + \dot{\theta}_3 (RS_Z - \theta_3 RS_X)] \end{aligned} \quad (B-7)$$

$$F_{13Z} = K_{TZ} (R_{1Z} - \theta_1 RH1_X + RH1_Z - R_{3Z} + \theta_3 RS_X - RS_Z) \\ - D_{TZ} [\dot{R}_{3Z} - \dot{\theta}_3 (RS_X + \theta_3 RS_Z)] \quad (B-8)$$

$$F_{32X} = K_{GX} (R_{3X} - R_{2X} + RH3_X + \theta_3 RH3_Z - \cos \theta_2 RH2_X \\ - \sin \theta_2 RH2_Z) + D_{GX} [\dot{R}_{3X} - \dot{R}_{2X} + \dot{\theta}_3 (RH3_Z \\ - \theta_3 RH3_X) - \theta_2 (\cos \theta_2 RH2_Z - \sin \theta_2 RH2_X)] \quad (B-9)$$

$$F_{32Z} = K_{GZ} (R_{3Z} - R_{2Z} - \theta_3 RH3_X + RH3_Z + \sin \theta_2 RH2_X \\ - \cos \theta_2 RH2_Z) + D_{GZ} [\dot{R}_{3Z} - \dot{R}_{2Z} - \dot{\theta}_3 (RH3_X \\ + \theta_3 RH3_Z) + \dot{\theta}_2 (\cos \theta_2 RH2_X + \sin \theta_2 RH2_Z)] \quad (B-10)$$

The rotational equations of the three bodies are as follows:

$$J_1 \ddot{\theta}_1 = -T_{13} - RH1_Z (F_{13X} - \theta_1 F_{13Z}) + RH1_X (\theta_1 F_{13X} \\ + F_{13Z}) + RF1_Z F_{1X} - RF1_X F_{1Z} \quad (B-11)$$

$$J_2 \ddot{\theta}_2 = T_M + RH2_Z (\cos \theta_2 F_{32X} - \sin \theta_2 F_{32Z}) \\ - RH2_X (\cos \theta_2 F_{32Z} + \sin \theta_2 F_{32X}) \quad (B-12)$$

$$J_3 \ddot{\theta}_3 = -T_M + T_{13} - RH3_Z (F_{32X} - \theta_3 F_{32Z}) \\ + RH3_X (\theta_3 F_{32X} + F_{32Z}) + RS_Z (F_{13X} \\ - \theta_3 F_{13Z}) - RS_X (\theta_3 F_{13X} + F_{13Z}) \quad (B-13)$$

where

$$T_{13} = K_R (\theta_1 - \theta_3) + D_R (\dot{\theta}_1 - \dot{\theta}_3) \quad (B-14)$$

$$\theta_E = \theta_C - \theta_2 \quad (B-15)$$

$$T_M = K_P \theta_E - K_1 \dot{\theta}_2 + K_I \int \theta_E dt \quad (B-16)$$

The experiment error ( $\theta_E$ ) was defined as the difference between the commanded attitude ( $\theta_C$ ) and the actual experiment attitude ( $\theta_2$ ). The experiment control torque was derived from a simple proportional, plus rate, plus integral control law.

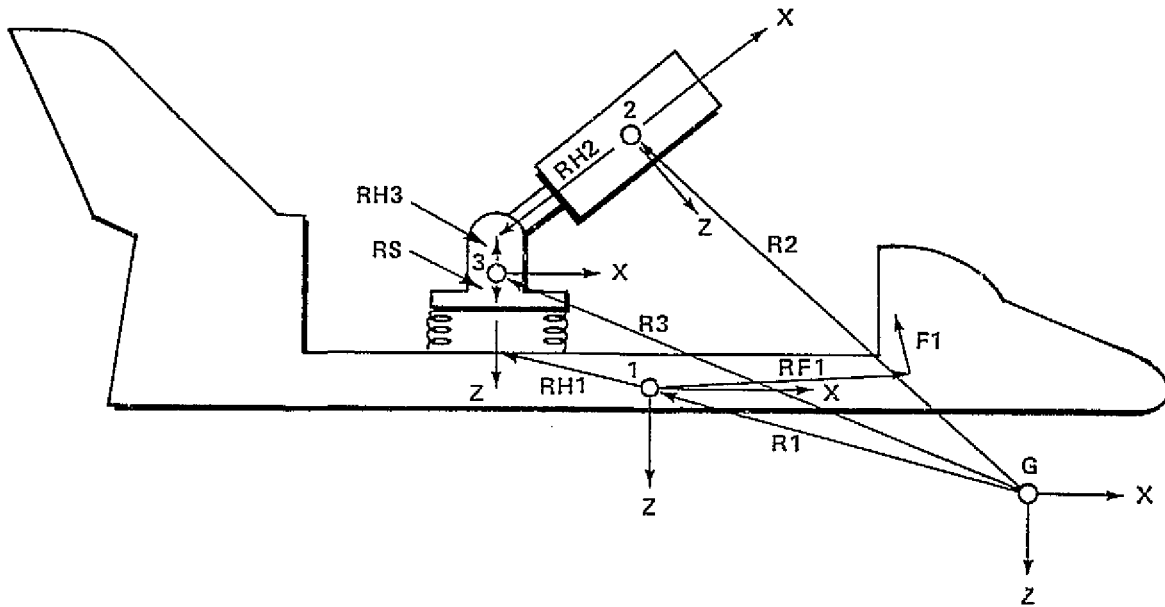


Figure B-1. Three-body planar model.

## APPENDIX C

### COMPUTER OUTPUT

The computer outputs presented in this appendix are chart recordings of various system dynamic variables. Considerably more information and insight into the dynamic behavior of the MPM can be obtained from the chart recording than from the summary charts contained in the main body of this report. Each column in the figures of this appendix represents a separate computer run and a different set of parameters to demonstrate the effect on the system dynamic response and performance. The control loop bandwidth was based on the inertia of the experiment, and no attempt has been made to optimize the control gains. The MPM was analyzed with both soft mounts and hard mounts between the Spacelab pallet and the MPM pedestal. Two sets of soft mounts, i.e., 100 N/m and 250 N/m for shock mount stiffness, and one hard mount set, i.e.,  $10^5$  N/m for shock mount stiffness, were used in the study. A brief discussion of the conditions and results of each set of computer runs is contained in the following paragraphs.

Figure C-1 shows the MPM dynamic response to a man motion disturbance for  $30^\circ$ ,  $60^\circ$ , and  $90^\circ$  pointing positions and 100 N/m shock mount stiffness between the pallet and MPM pedestal. The man motion described in Figure V-3 was applied 15 m forward of the Shuttle/pallet center of mass in both the X and Z directions simultaneously. The MPM was mounted on the Spacelab pallet 10 m forward of the Shuttle/pallet center of mass. The control loop bandwidth was approximately 3 Hz based on the small instrument characteristics, i.e., the 130 kg Schwarzschild camera. Figure C-1 demonstrates the effect of pointing position on stability (THETA2), stability rate (THETA2D), and control torque (TM). Figure C-2 shows the dynamic response for a 250 N/m shock mount stiffness with all other parameters the same as in Figure C-1. This stiffer soft mount resulted in slightly larger magnitudes of stability, stability rate, and control torque.

Figure C-3 shows the effect of hard mounting the MPM to the Spacelab pallet. The hard mount was represented by a  $10^5$  N/m shock mount stiffness. The control loop bandwidth was reduced to 0.5 Hz to stabilize the control loop and reduce control torque. All other parameters remained the same as in Figure C-1. The values of stability, stability rate, and control torque were much larger than for the soft mounted MPM shown in the previous figures.

Figures C-4, C-5, and C-6 depict the dynamic responses similar to those in Figures C-1, C-2, and C-3. Figures C-4, C-5, and C-6 represent the large instrument, i.e., a 500 kg experiment, whereas Figures C-1, C-2, and C-3 represent the small instrument.

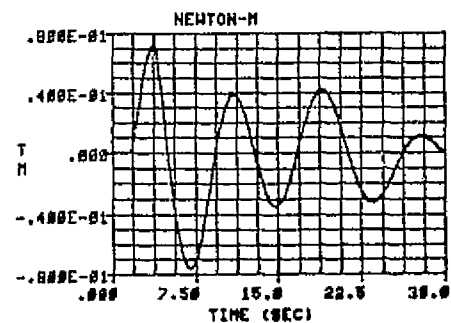
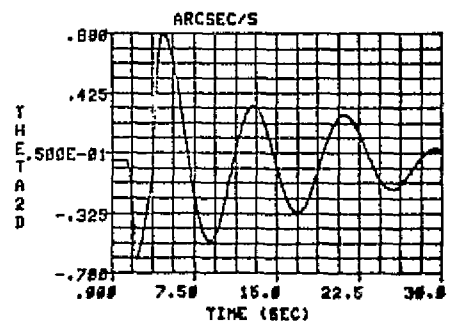
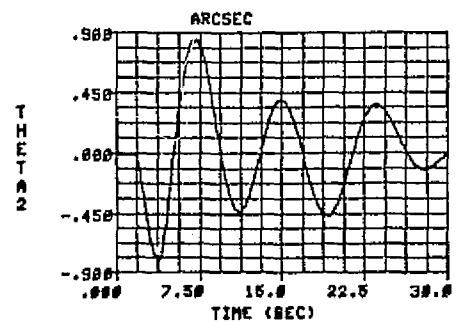
In Figure C-4 the control loop bandwidth was approximately 3 Hz based on the large instrument characteristics, and the shock mount stiffness was 100 N/m. Comparing Figure C-4 with Figure C-1 shows much less stability error and only a small increase in control torque. The smaller stability error was primarily attributed to greater disturbance attenuation for larger experiments. The periods of the dynamic responses were considerably longer for the larger instrument. Figure C-5 shows the dynamic responses for a shock mount stiffness of 250 N/m with all other parameters the same as in Figure C-4.

In Figure C-6 the MPM with large instrument was hard mounted to the pallet. The hard mount was represented by a shock mount stiffness of  $10^5$  N/m and the control loop bandwidth was set at 0.5 Hz. All other parameters were the same as for Figure C-4. Again the stability, stability rate, and control torque were much larger than for the soft mounted MPM with the large instrument shown in Figures C-4 and C-5.

Figures C-7 and C-8 illustrate the dynamic performance of the MPM while tracking an earth surface target. The MPM was soft mounted with a 100 N/m shock mount stiffness. A slow and a fast tracking profile were simulated with maximum tracking rates of  $1.0^\circ/\text{s}$  for approximately 470 km altitude and  $1.5^\circ/\text{s}$  for approximately 310 km altitude, respectively. THETA2 represents the angular motion and THETA2D is the angular rate of the experiment package. THETA E represents the angular error between the target line of sight and the actual line of sight of the experiment. TM represents the control torque. The total angular range of THETA2 was  $130^\circ$ , i.e.,  $25^\circ$  to  $155^\circ$ .

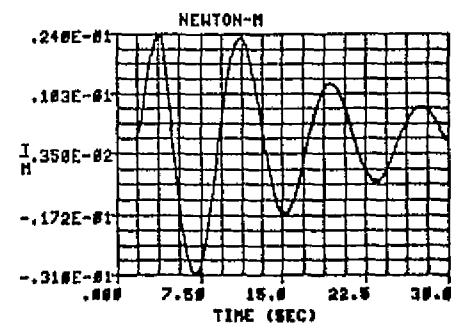
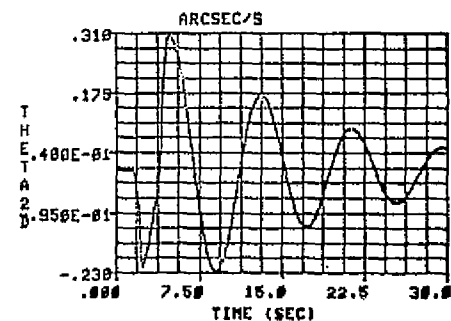
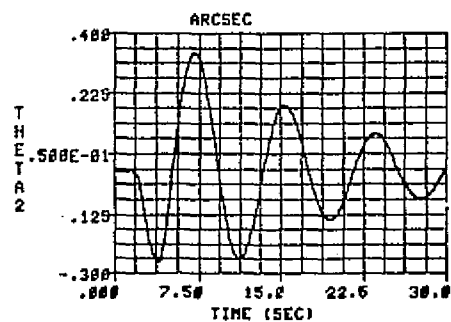
Figure C-7 represents the small experiment and Figure C-8 represents the large experiment tracking an earth surface target for altitudes as follows: (1) 470 km with a peak tracking rate of  $1.0^\circ/\text{s}$ , and (2) 310 km with a peak tracking rate of  $1.5^\circ/\text{s}$ . In all cases the peak control torque was less than the MPM maximum torque capability, and the peak tracking error was less than 1 arc s. The simulation assumed an ideal target sensor.



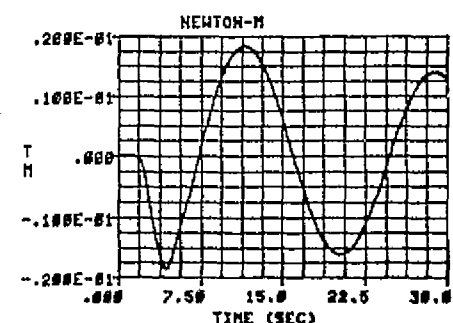
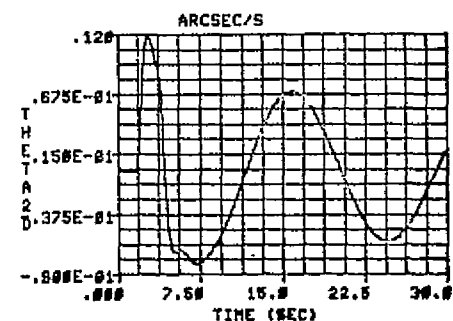
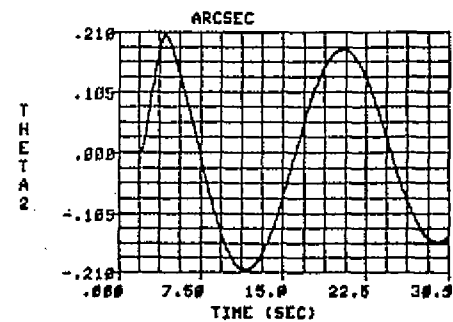


POINTING  
POSITION (deg)

30



60



90

Figure C-1. Dynamic response for 100 N/m shock mount stiffness.

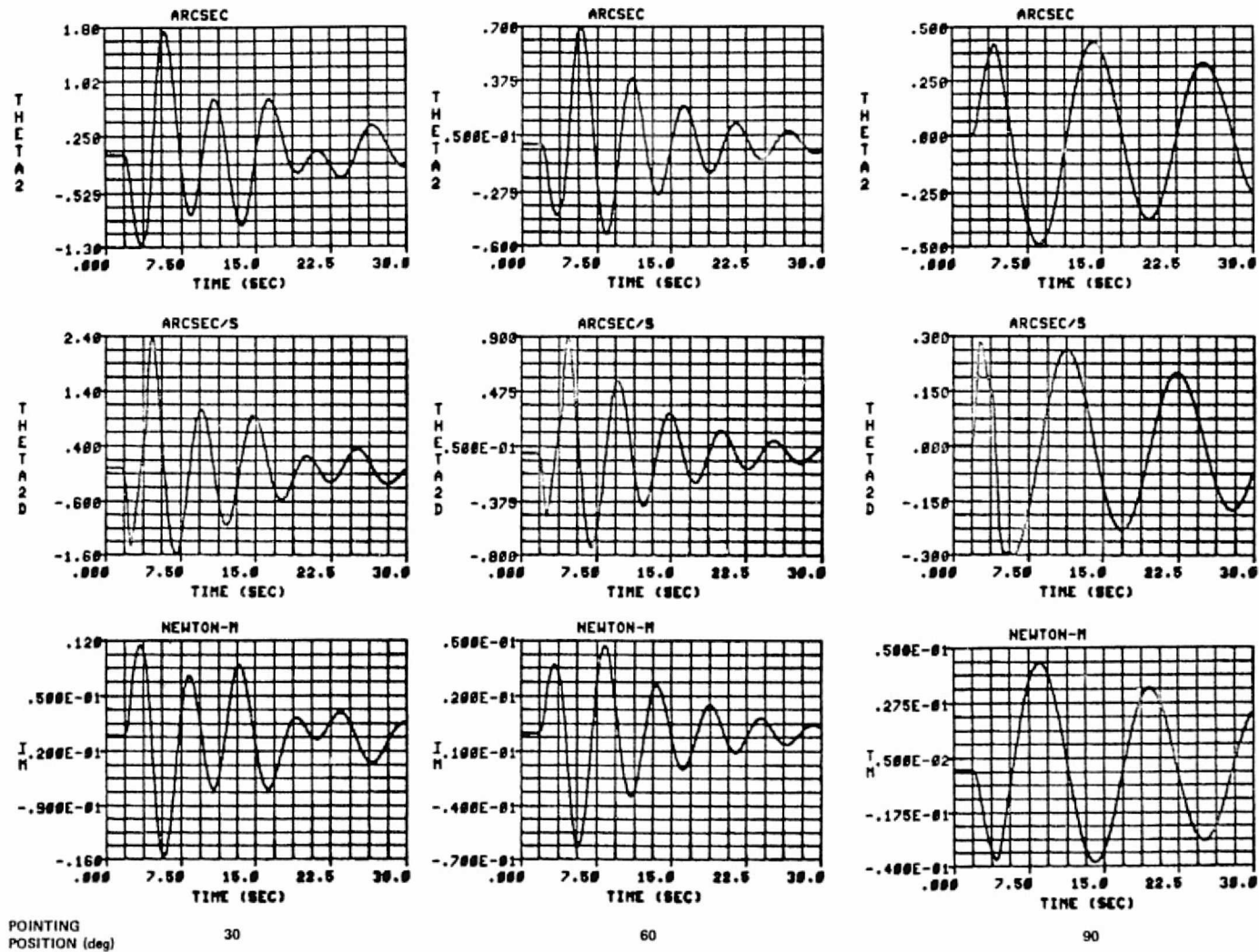


Figure C-2. Dynamic response for 250 N/m shock mount stiffness.

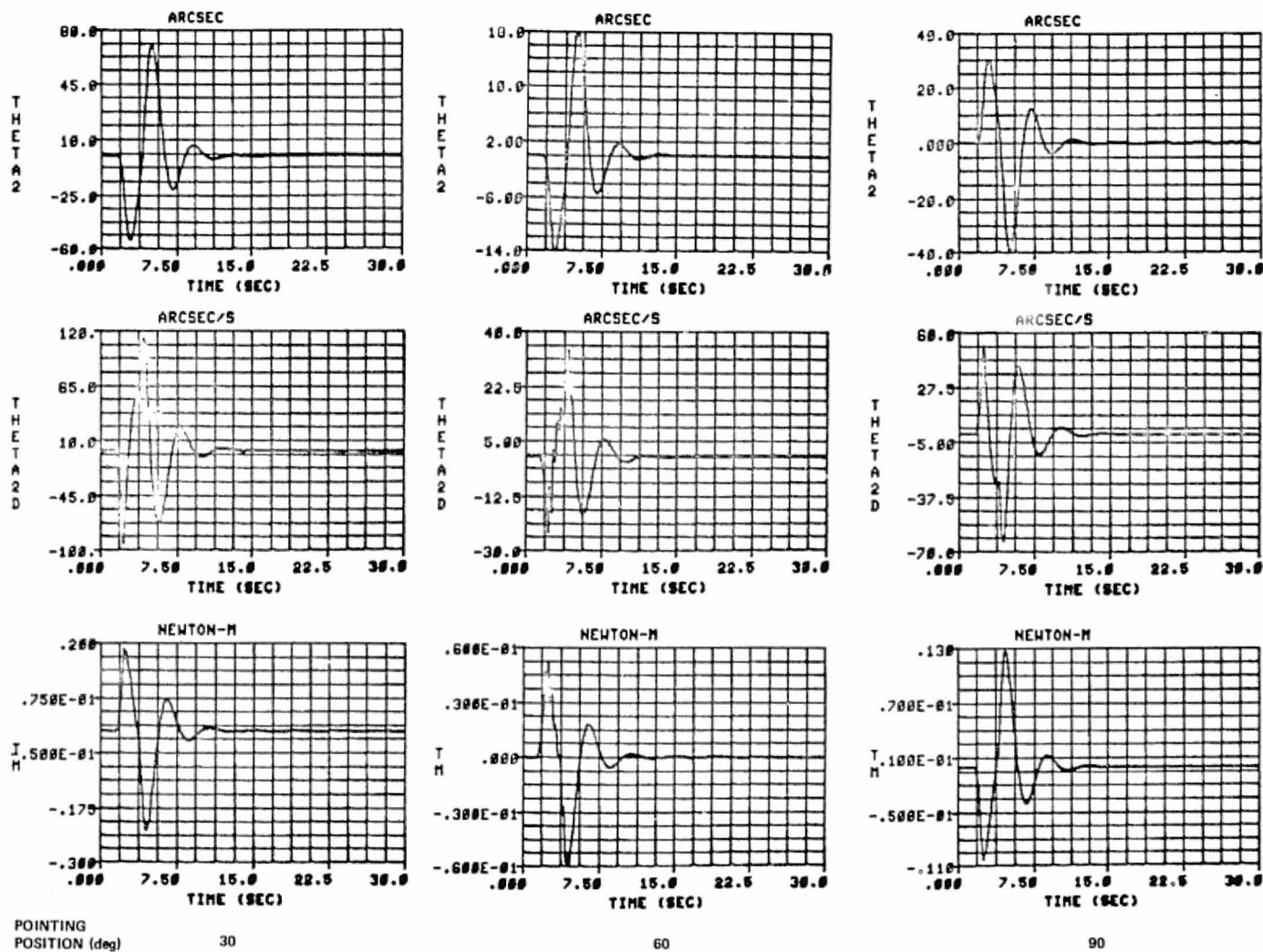


Figure C-3. Dynamic response for  $10^5$  N/m shock mount stiffness.

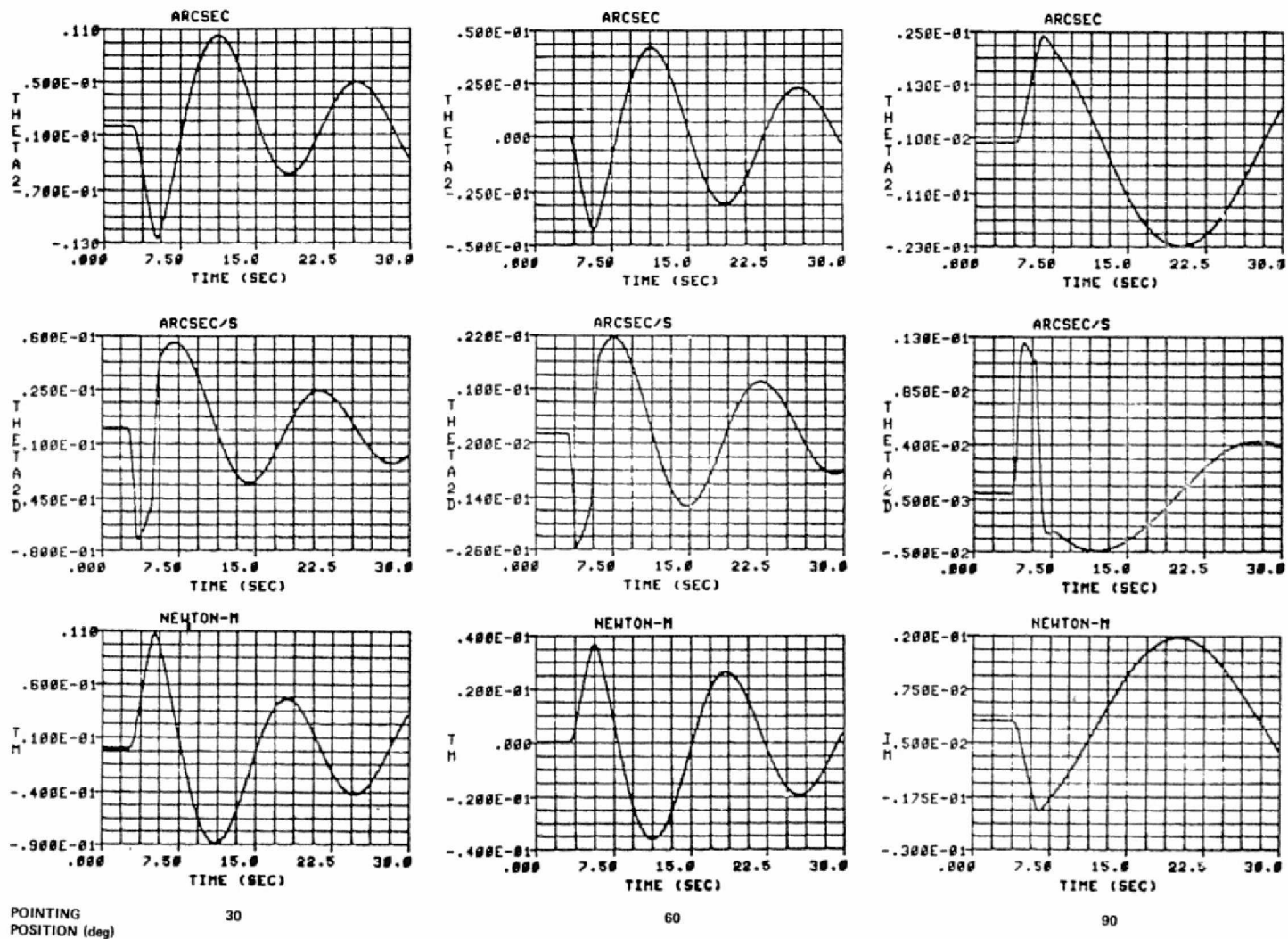
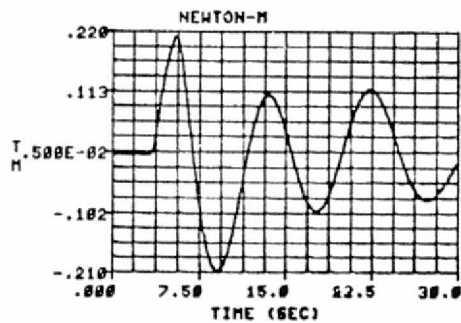
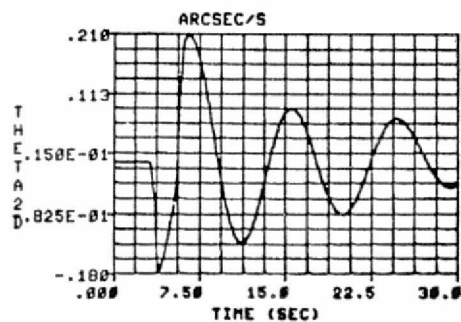
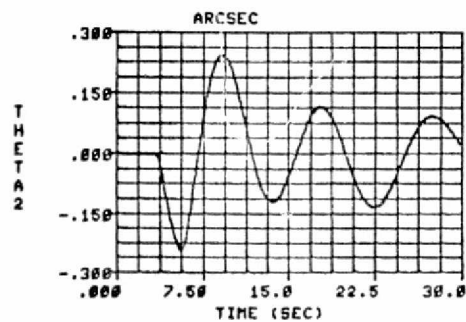
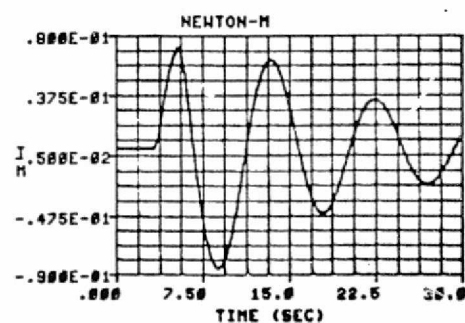
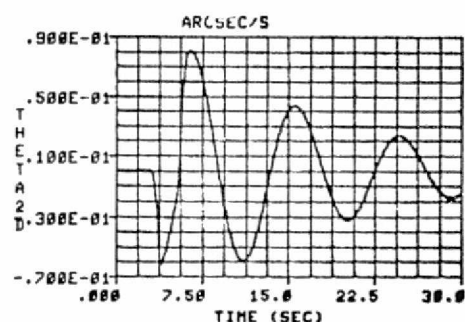
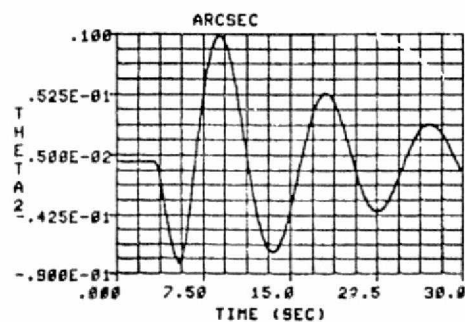


Figure C-4. Dynamic response for 100 N/m shock mount stiffness.

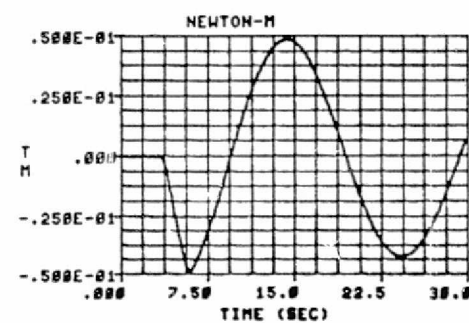
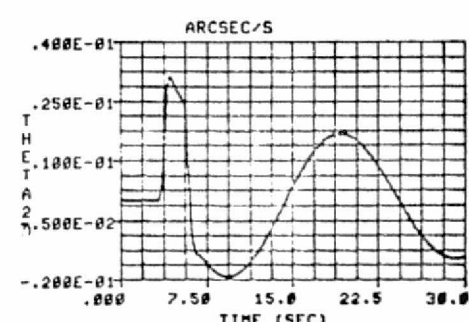
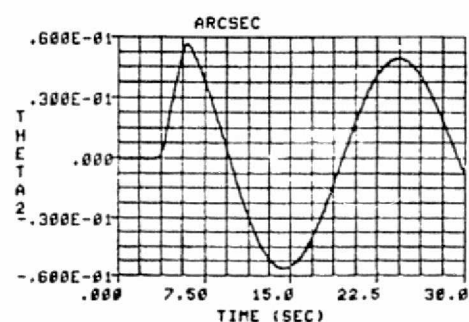


POINTING  
POSITION (deg)

30



60



90

Figure C-5. Dynamic response for 250 N/m shock mount stiffness.

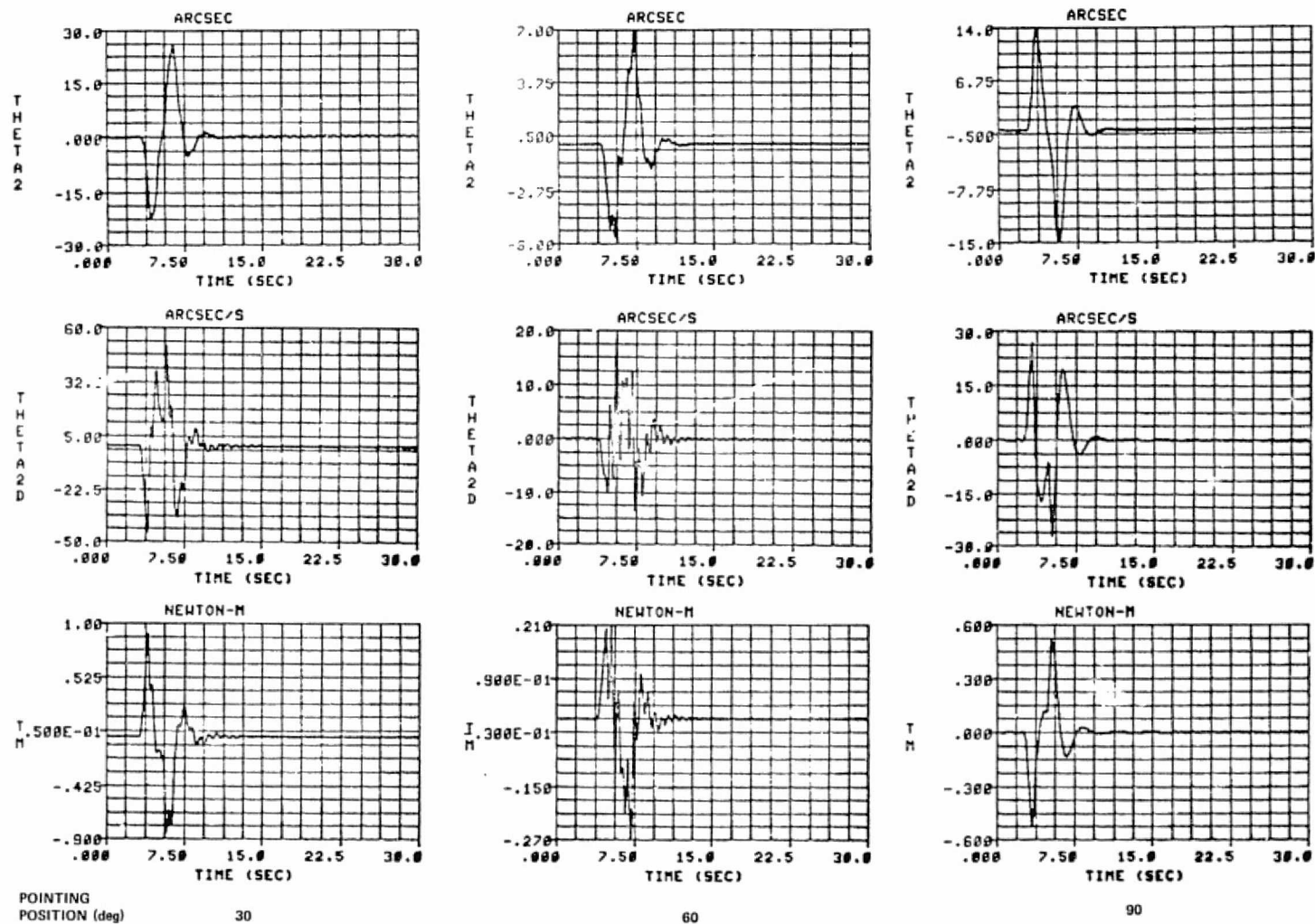
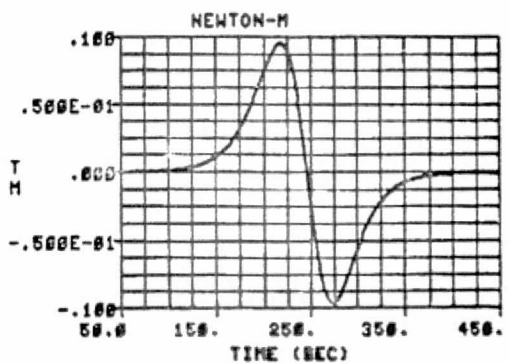
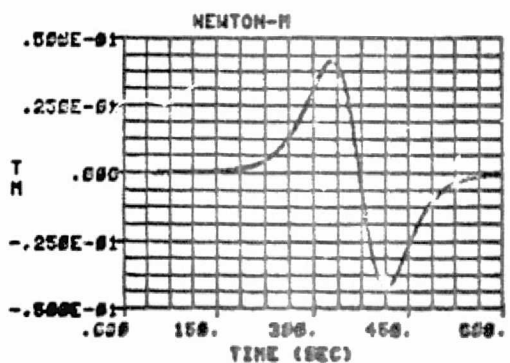
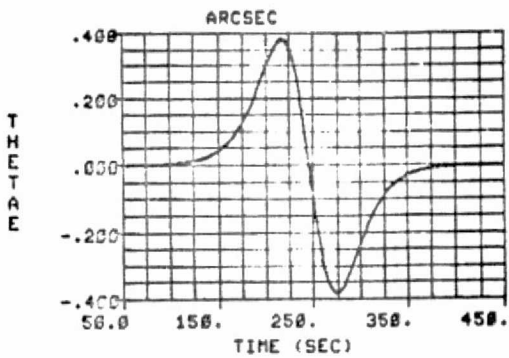
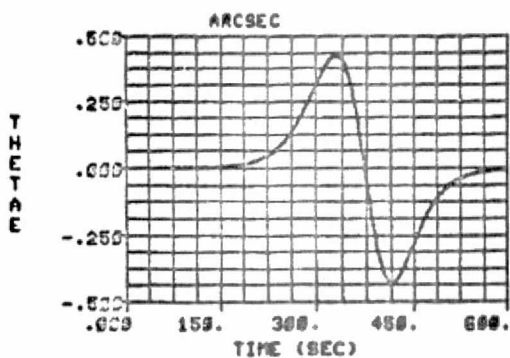
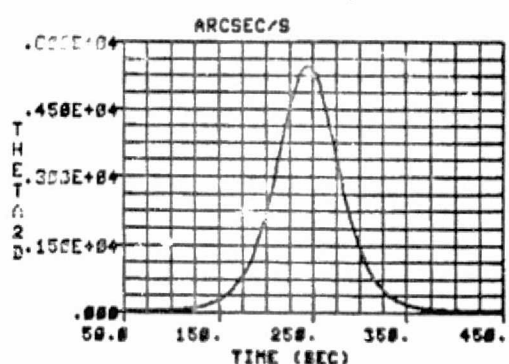
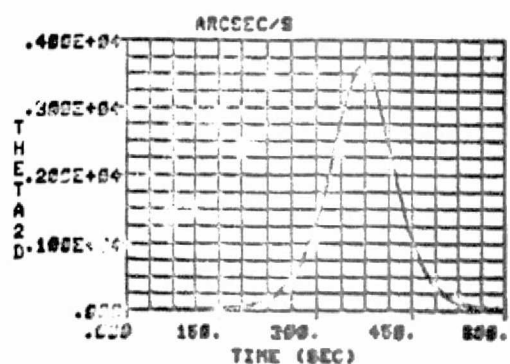
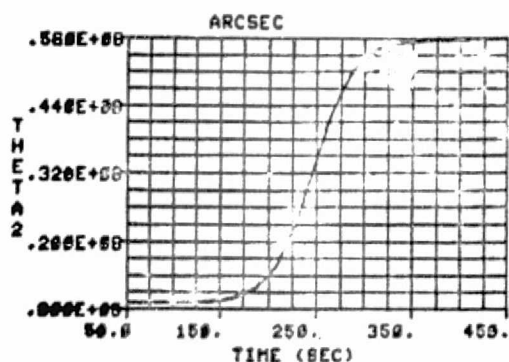
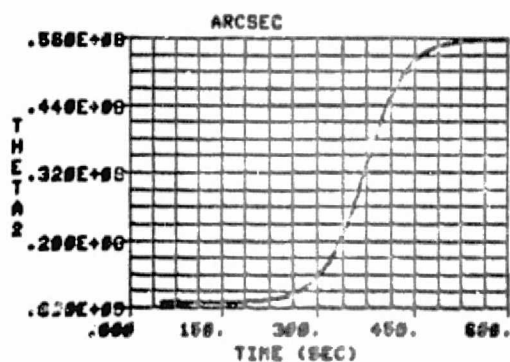


Figure C-6. Dynamic response for  $10^5$  N/m shock mount stiffness.

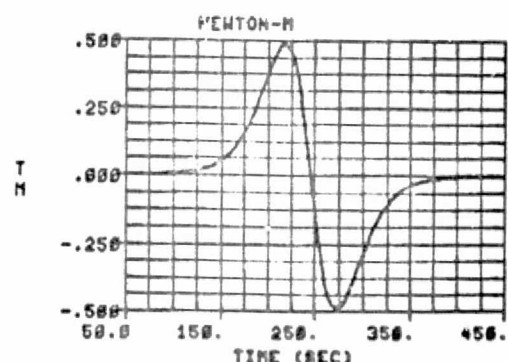
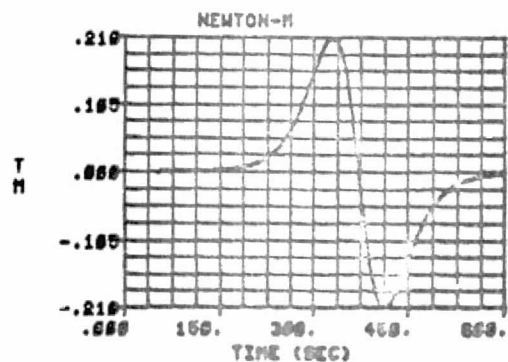
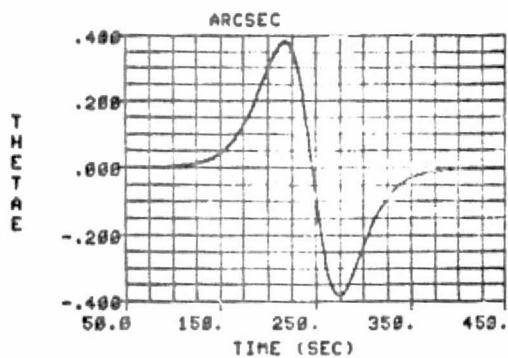
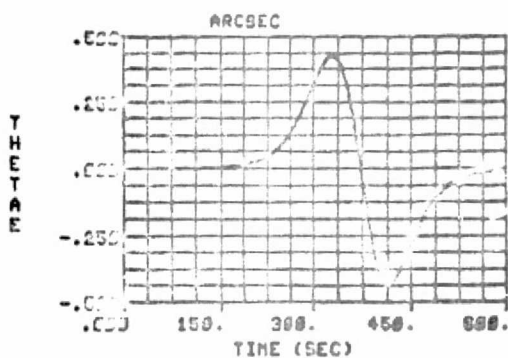
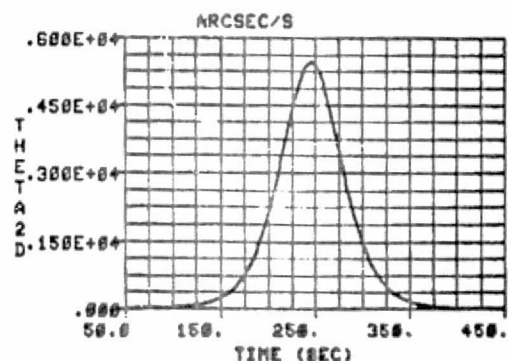
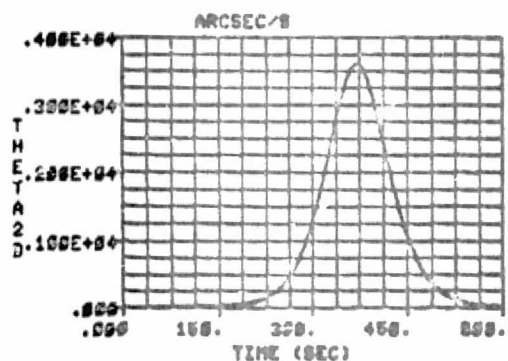
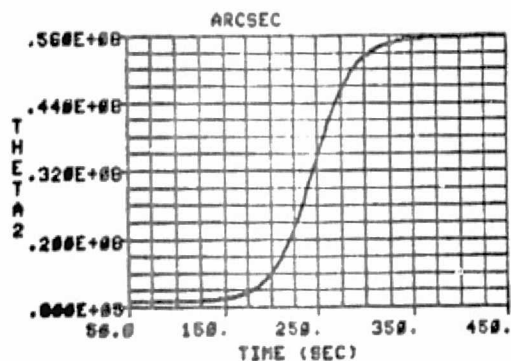
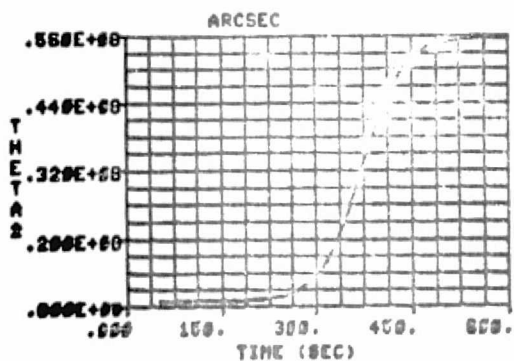


(a)

(b)

Figure C-7. Slow and fast tracking for the small experiment.





(a)

(b)

Figure C-8. Slow and fast tracking for the large experiment.



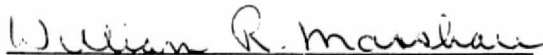
## APPROVAL

### A MINIATURIZED POINTING MOUNT FOR SPACELAB MISSIONS

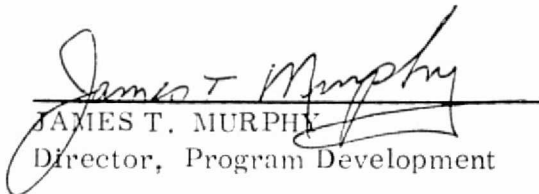
By Carl G. Fritz, Joe T. Howell, Jr.,  
P. D. Nicaise, and Joe R. Parker

The information in this report has been reviewed for security classification. Review of any information concerning Department of Defense or Atomic Energy Commission programs has been made by the MSFC Security Classification Officer. This report, in its entirety, has been determined to be unclassified.

This document has also been reviewed and approved for technical accuracy.



WILLIAM R. MARSHALL  
Director, Preliminary Design Office



JAMES T. MURPHY  
Director, Program Development